The Electronic Structure of Bilayer $MoSe_2$ of AB and AA Stacking order under various External Electric Field and Biaxial strain values

By

ARPITA NANDI

Registration No. **150129** of 2019-2020

Examination Roll No. **M6VLS22001**

Under the Guidance of

Dr. Divya Somvanshi

Thesis Submitted in partial fulfilment of the requirement for the award of the Degree of Master of Technology in VLSI Design and Microelectronics Technology

Department of Electronics & Telecommunication Engineering

Kolkata-700032

West Bengal, India

JUNE 2022

Faculty of Engineering & Technology
Jadavpur University

CERTIFICATE OF RECOMMENDATION

I hereby recommend that this thesis prepared by **Arpita Nandi** entitled "**The Electronic Structure of Bilayer $MoSe_2$ of AB and AA Stacking order under various External Electric Field and Biaxial strain values"** under my supervision be accepted for partial fulfillment of the requirements for the award of the Degree of Master of Electronics and Telecommunication Engineering.

……

Dr. Divya Somvanshi
Thesis Supervisor
Department of Electronics and Tele-Communication Engineering
Jadavpur University, Kolkata – 700032

……

Dr. Ananda Shankar Chowdhury
Professor and Head of the Department
Department of Electronics and
Tele-Communication Engineering,
Jadavpur University, Kolkata – 700032

……

Prof. Chandan Mazumdar
Dean
Faculty Council of Engineering and Technology
Jadavpur University, Kolkata – 700032

FACULTY OF ENGINEERING & TECHNOLOGY

JADAVPUR UNIVERSITY

DEPARTMENT OF ELECTRONICS &
TELECOMMUNICATION ENGINEERING

CERTIFICATE OF APPROVAL*

The foregoing thesis is hereby approved as a credible study of an Engineering subject and presented in a manner satisfactory to warrant acceptance as pre-requisite to the degree for which it has been submitted. It is understood that by this approval the undersigned do not necessarily endorse or approve any statement made, opinion expressed or conclusion drawn therein but approve the thesis only for which it is submitted.

Committee on final examination
For the evaluation of the Thesis of

Arpita Nandi

External Examiner

Dr. Divya Somvanshi

Department of Electronics &
Telecommunication Engineering
Jadavpur University
Kolkata-700032.

*****Only in case the thesis is approved.

FACULTY OF ENGINEERING & TECHNOLOGY

JADAVPUR UNIVERSITY

DECLARATION OF ORAGINALITY AND COMPLIANCE OF ACADEMIC ETHICS

It is hereby declared that this thesis entitled **"The Electronic Structure of Bilayer $MoSe_2$ of AB and AA Stacking order under various External Electric Field and Biaxial strain values"** contains original research work by the undersigned candidate, as a part of his degree of **Master of Technology in VLSI Design & Microelectronics**.

All information has been obtained and presented in accordance with academic rules and ethical conduct.

It is also asserted that, as required by these rules and conduct, the undersigned has fully cited and referenced all materials and results that are not original to this work.

Name: ARPITA NANDI

Examination Roll No.: M6VLS22001

Thesis Titles: "The Electronic Structure of Bilayer $MoSe_2$ of AB and AA Stacking order under various External Electric Field and Biaxial strain values".

Date: **Signature of the candidate**

ACKNOWLEDGEMENTS

The success and final outcome of my thesis required a lot of guidance and assistance from many people and I am extremely fortunate to have got this all along the completion of my thesis work. Whatever I have done is only due to such guidance and assistance and I would not forget to thank them.

First and foremost, I owe my profound gratitude to my project supervisor, **Dr. Divya Somvanshi** who guided me till the completion of my project work by providing his precious advices and constant support. I would like to express my special appreciation and thanks to him for giving his full effort in guiding me to maintain the progress. They have been a tremendous mentor for me because without his invaluable suggestions and his continued motivation, my project work would not have taken a worthwhile shape.

I am thankful to and fortunate enough to get such a nice support, devotion and constant encouragement from my senior Mrs. Sayantika Chowdhury throughout my thesis work. She supported me in guiding, inspired me to strive towards my goal.

I would like to thank H.O.D Department of Electronics & Telecommunication Engineering, Jadavpur University by providing me all the facilities for carrying out the entire project work. I would like to express my sincere appreciation to all the teaching and non-teaching staff of the department for providing necessary support and aids.

Last but not the least, a special heartfelt thanks to my beloved family. Words cannot express how grateful I am to my parents for all of the sacrifices that they have made on my behalf. Their prayer for me was what sustained me thus far.

_____

Arpita Nandi

Date:

Place: Kolkata

TABLE OF CONTENTS

LIST OF FIGURES

Chapter-4

Chapter-5

LIST OF TABLES

ABSTRACT

Two-dimensional (2D) Materials are crystalline materials consist of a single layer of carbon atoms with thickness of few nanometers or lower. 2D materials having various properties such as high carrier mobilities, excellent conductivity, mechanical flexibility, good thermal conductivity and high optical and Ultraviolet (UV) adsorption. In $MoSe_2$ (Molybdenum diselenide), the 'Mo' atoms occupy one type of sub-lattices of the hexagonal sheet and atoms of 'Se' occupy the others. Chemical component in $MoSe_2$ (Ratio) is Mo: Se is equal to 1:2, the sub-lattice layer of 'Mo' is sandwiched between two nearby 'Se' sub-lattice layers. $MoSe_2$, a transition metal dichalcogenides (TMDCs), has gained considerable attention later on for various applications in optoelectronic systems, electrochemical and photocatalytic. In this work, we analyzed the effect of external electric field and biaxial strain on the electronic structures of AB and AA stacking bilayer (BL) $MoSe_2$ by using the density functional theory (DFT) calculations. Here we demonstrate an approach that the van der Waals (vdW) homo bilayer built by two monolayer $MoSe_2$ has a well-controlled electronic property with applied E-field. Results show that AB stacking bilayer $MoSe_2$ has an indirect band structure with the gap value of 1.09 eV whereas, the AA stacking bilayer $MoSe_2$ has an indirect band structure with the gap value of 1.25 eV. The band gap of AB stacking bilayer $MoSe_2$ decreases monotonically from the maximum (1.09 eV) at 0.0 V/Å to 0 eV at 2.8 V/Å in both, positive and negative direction along the z-axis. So, AB stacking bilayer $MoSe_2$ have been shown to have vastly different electronic behavior, ranging from semiconductor material to metallic material, when we applied external Electric field. On other side for AA stacking bilayer $MoSe_2$, bandgap decreases from the maximum (1.25 eV) at 0.0 V/Å to 0 eV at 2.2 V/Å in both, positive and negative direction along the z-axis. That means AA stacking bilayer $MoSe_2$ have been also shown different electronic behavior, ranging from semiconductor material to metallic material. Recent theoretical and experimental investigations have demonstrated flexible control over their electronic states via application of external strains, such as uniaxial strain and biaxial strain. Here, we determined that the critical biaxial strain range within the bandgap of AB and AA stacking $MoSe_2$ BL remains indirect upon application of ε from +7% to -7% (for AB) and +6% to -6% (for AA). Also, we have compared the rate of bandgap tunability of $MoSe_2$ BL for all possible bandgap transition routes. We strongly believe that results of this analysis will help possible applications and modeling based on $MoSe_2$ BL for future integrated electronic and optoelectronic device applications.

Chapter 1

INTRODUCTION

1.1 2D Materials

Two-dimensional (2D) materials are crystalline materials consisting of a single layer of atoms with thickness of few nanometers or less [1, 2]. Electrons in 2D materials can be moved freely in 2D plane but restricted to 3D which is governed by quantum mechanics. Prominent examples include quantum wells and graphene [3]. First 2D material graphene was discovered in 2004 by two researchers at the University of Manchester, Prof. Andre Geim and Prof. Kostya Novoselov [3]. They used the scotch-tape method to separate a single layer of graphene from graphite. After that several 2D materials have been discovered like black-Phosphorus (BP), MoS_2, h-BN, etc. [4]. Many of 2D materials have been predicted and discovered by using theoretical methods, mainly DFT (density functional theory) calculations but most of these discoveries were done by trial-and-error experimental synthesis [5]. The discovery of MXene was taken place in 2011 at Drexel University. 2D materials can be classified mainly into four types, those are graphene, TMDC, h-BN, BP [6]. In this four materials graphene has zero band-gap due to which it behaves as a semimetal. Insulating hexagonal boron nitride (hBN) behaves as an insulator with bandgap around ~ 6 eV [7]. BP has lower effective mass than TMDC's due to which it has high ON current. In spite of having above advantages BP shows less stability as compared to other TMDC's [8]. The last member of this family is semiconducting TMDC materials (MoS_2, $MoSe_2$, WSe_2, WS_2, $SnSe_2$ etc.) which has tunable bandgap (1.2 eV to 2.5 eV) which is attractive for optoelectronics application [9]. Due to those tunable bandgaps of TMDC it shows semiconducting properties [10]. 2D materials have emerging applications in electronics industry like sensing, spintronics, plasmonics, photodetectors, ultrafast lasers, batteries, supercapacitors, and thermoelectric [11].Among the above, TMDCs are more promising for switching applications due to its band gap and stability over Graphene and Phosphorene respectively [12].

1.2 TMDC Materials

Transition metal dichalcogenides (TMDCs) are a part of vast 2D materials community , which are explored for various next-generation electronics and optoelectronics applications [13]. These TMDC materials have attracted tremendous attention because of the special structural features such as layer dependent bandgap, atomic thickness, excellent mechanical, and thermal stability and find their tremendous applications in optoelectronics, electronics, mechanical, optical, photocatalysis, and energy-storage applications [14]. TMDC materials are formulated as X–M–X, is a plane of transition metal atoms (M) (such as molybdenum (Mo) or tungsten (W)) within the groups 4 to 10 of the periodic table covalently sandwiched by two hexagonal planes of chalcogen atoms (X) (such as sulfur (S), selenium (Se) or Tellurium (Te)) from group 16 of the periodic table [15]. Highlighted element in sky blue on the periodic table shown in Fig:1.1 indicates the transition element and dark yellow indicates chalcogen elements. The TMDCs materials are bonded by strong in-plane covalent bonds and weak out-of-plane van der Waals (vdW) forces. This kind of unique structural characteristics give unique properties to TMDCs materials.

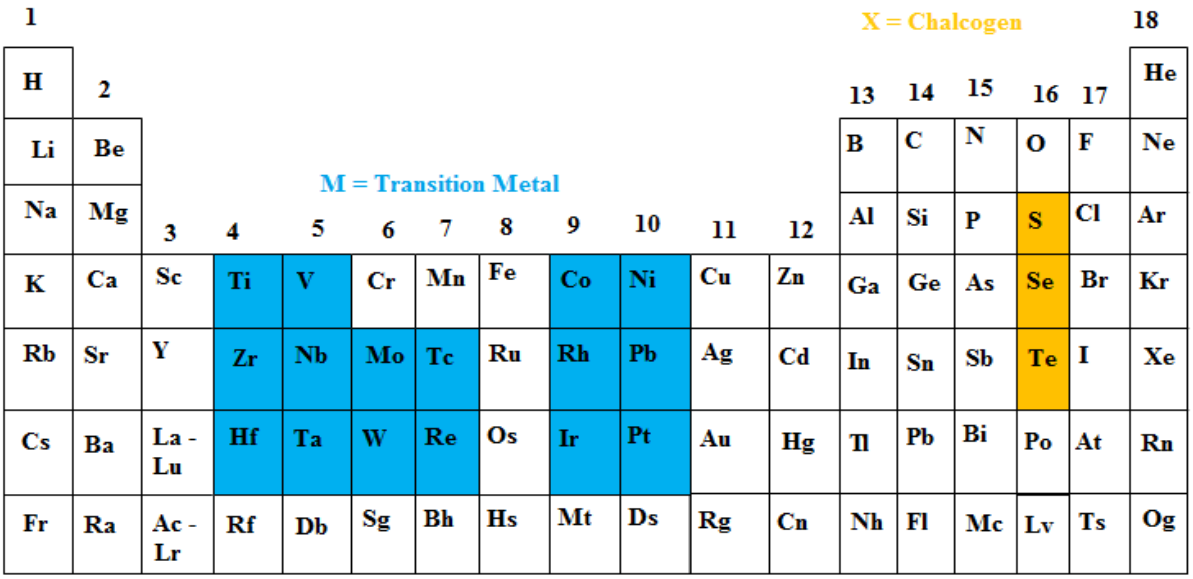

Fig: 1.1 Periodic table of elements presenting the possible combinations of elements forming layered TMDCs MX_2 [16].

The different stacking of the layers along c-axis determines polymorphic crystal structures within TMDCs, and also the common phases are 1T, 2H, 3R, and Td phases (T—trigonal, H—hexagonal, R—rhombohedral, and Td—distorted octahedral) [17].

There are more than 40 different TMDC materials types, which includes metals (such as TiS_2 and VSe_2), superconductors (such as TaS_2 and NbS_2), semimetals (such as $MoTe_2$ and WTe_2), and semiconductors (MoS_2, $MoSe_2$, WS_2, and WSe_2) [18]. TMDCs have been shown interesting band structures with tunable bandgaps. For example, graphene is a semimetal material with zero bandgap, which limits its application in electronics and photo-electronics [7]. TMDCs exhibit variable bandgaps from 0 to 2 eV, which can further modified by various factors like, defects, dopants, external electric field and mechanical deformations (by applying the tensile strain or compressive strain) [19].

TDMCs can exhibit unique structural conformations due to the different spherical coordination of the transition metal atoms. Among them, most common polymorphs are octahedral (1T) and trigonal prismatic (2H and 3R) (Figure 1.2).

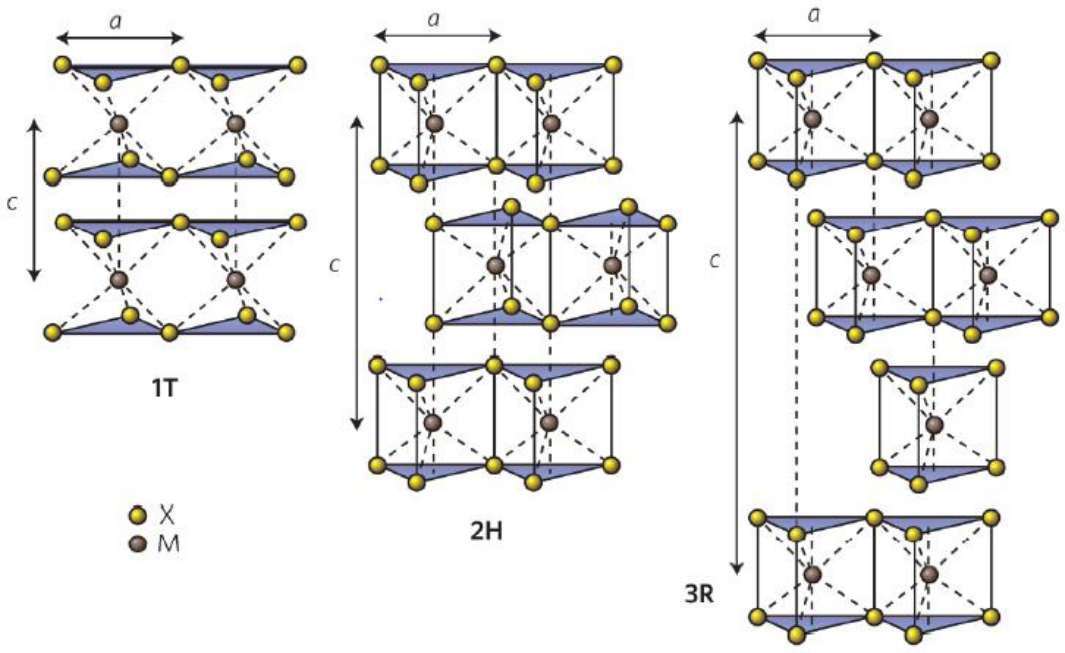

Figure 1.2 Schematics of the crystalline structures of 1T, 2H, 3R phases of TMDCs [20].

1.3 Bilayer TMDC and their Stacking order

A bilayer is a structure consisting of two layers, it may be homo bilayer which composes of two similar or different (Hetero) type of monolayer TMDC. For homo- bilayers, in general we considered same type of materials (E.g., MoS_2-MoS_2, WS_2-WS_2, $MoSe_2$-$MoSe_2$, WSe_2-WSe_2 etc.). For hetero-bilayers, we have considered different type of monolayer TMDC materials (E.g., $MoSe_2$-WS_2, WSe_2-MS_2, $MoTe_2$-MoS_2 etc.).

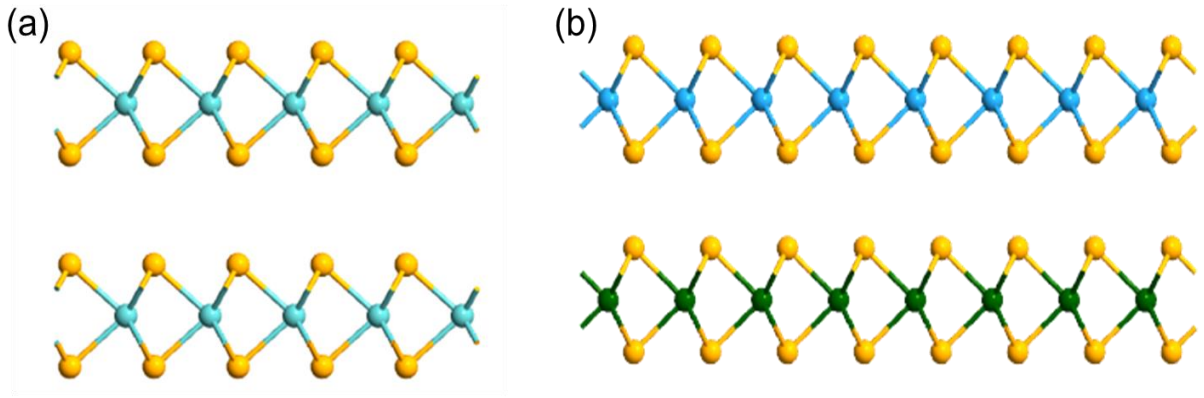

Fig 1.3: Bilayer TMDCs- (a) Homo bilayer TMDC ($MoSe_2$), (b) Hetero bilayer TMDC MSe_2 (M= Mo, W)

As compare to monolayer, the bilayer TMDCs have an additional degree of freedom, such as stacking orders, twist angle, and heterostructures. Here, we will be discussing about the possible contribution of different stacking order i.e., how the monolayers are arranged with respect to each other towards the formation of the homo bilayers. We are mainly focused on the two most important stacking order i.e., AA and AB. In AB stacked bilayer, the Mo atoms from the second layer are directly above the Se atoms from the first layer, while for the AA stacking, the Mo atom from the first layer is directly above on the second Mo atom of second layer. Fig. 1.4 shows the schematic atomic structure of bilayer AB and AA stacked $MoSe_2$.

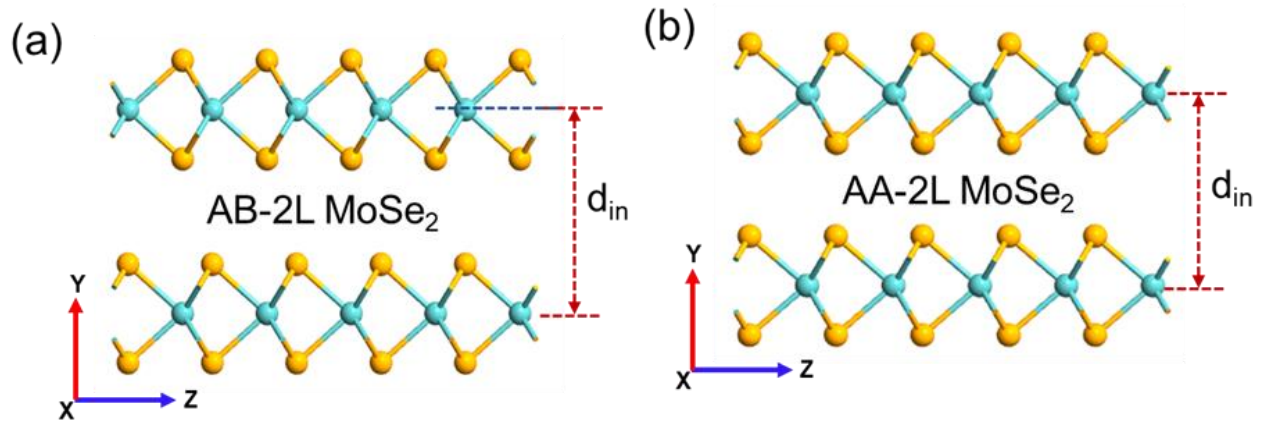

Fig.1.4 Schematic atomic model of the 2L $MoSe_2$ (a) AB stacking (b) AA stacking, where d_{int} is the interlayer distance between Mo-Mo; the light blue and orange bolls denote the Mo and Se atoms.

1.4 Mechanical Strain

Mechanical strain represents a geometrical degree of distortion, which represents the relative displacement between particles in different materials system. There are various ways by which strain can be applied in a material system, the details are given below:

A) ***Longitudinal Strain*****:** When the distortion force on the materials system produces a change along the length given body in the direction of force, then the strain created within the body is known as Longitudinal strain. It is equal to the ratio of modification in length of a body to its original length. It can be categorized into two different categories:

i> ***Tensile strain***: - It is described as the distortion or extension of a materials system because of the application of a mechanical stress. In other words, when in materials system upon application of force, there is increase in length of the body or when applied force attempt to stretch it, the tensile strain is created. It can be mathematically expressed by the following relation formula:

$$\varepsilon = \Delta L / L,$$

where, ε = Tensile strain,

ΔL = Change in length and

L = Original length

ii> ***Compressive strain***: - It is described as the distortion or contraction in a materials system because of the application of mechanical stress. In other words, when the mechanical stress is applied, then there is contraction in the materials length or mechanical forces attempt to compress it. This is also the reason, the compressive strain also called as negative strain. Mathematically, it can be expressed by ratio of the object's change in length to its original length. It can be mathematically expressed by the following relation formula:

The formula for compressive strain is:

$$e = \Delta L / L$$

where: e = compressive strain, ΔL = change in length and L = original length

B) ***Lateral Strain****:* When the distortion force produces an alteration along the length of the given materials system perpendicular to the direction of mechanical force, then a mechanical strain is produced that is called Lateral strain.

C) ***Volumetric Strain*****:** When the distortion force produces a change in volume of the given materials system, then the produced strain is called volumetric strain. It is equal to the ratio of modification in volume of a materials system to its original volume of material.

D) ***Shearing Strain****:* When the distortion force produces a change in the overall shape of a materials system without any change in its volume, then the mechanical strain is produced known as the Shearing strain. Basically, it is the angular displacement of the plane of a materials system perpendicular to the fixed surface.

➢ External Electric Field

External Electric field can be applied to given materials system in a various ways considered as an electric property related with each point in the space where a charge is present in any form.

In 2D semiconductors, external E-field have a profound effect. In bilayer graphene, it can open the band gap, where as in bilayer InSe and MoS_2, it can reduce the bandgap or for higher E- field

semiconductor to metallic transition is observed. Therefore, in this thesis, we also explored effect of external E field also on electronic structure of AB and AA stacked bilayer $MoSe_2$.

1.5 Density Functional Theory (DFT)

Density Functional Theory (DFT) is a computational technique and, vastly used to study electronic structure and optical properties of nanomaterials, surfaces, interface etc. by directly solving many atom versions of Schrödinger equation using various approximations. Basically, DFT calculations, are using ab initio methods from first principles calculations which permit the prediction and calculation of various material properties based on quantum mechanical calculations [21-23].

- DFT was first theoretically introduced by **Walter Kohn and Pierre Hohenberg** in 1964, which states that The Ground state energy E is a unique functional of the electron density: (Hohenberg and Kohn, 1964)**,**

  $$\mathbf{E = E\,[n(r)]}$$

- Later, **Kohm and Sham** in in 1965 states that the electron density that minimizes the energy of the overall functional is the true ground state electron density**.** (Kohn and Sham, 1965)

  $$\mathbf{E\,[n(r)] > E_0\,[n_0(r)]}$$

However, DFT gone through the a very long evaluation with time, initially, before 1980, it was not considered precise enough for calculations in quantum chemistry. However, in 1980's, when the various approximations such as to calculation of the coulombic interactions were introduced and it was and critically polished through the years to offer better modelling of the exchange and correlation interactions.

In 1966, Phillips and Kleinman described that the electrons in any solids is constrained to the outer most valance shell, which was achieved by replacing the nuclear potentials by ionic pseudopotentials. Later, in 1979, ionic pseudopotentials were directly combined within DFT, which led the path to perform the first principal calculations without the core electrons, which makes them much faster than the earlier calculations. In 1989, various new algorithms were introduced by using linear algebra techniques to improve the studies for large systems in order to

solve Kohn-Sham equations more competently. Further, in early 1990's, soft pseudopotentials, projected augmented wave (PAW) and linear-scaling DFT calculations were introduced and developed to make the computations for very large systems both cost effective and faster. In 1991, various new corrections ware also developed and introduced such as Hubbard-corrected density functional theory and DFT-1/2 corrections were to obtain accurate band gaps in many materials including semiconductors. Even now today, researchers all around the globe are working relentlessly, to making DFT computations more practical and advanced [24].

1.5.1 Significance of DFT

DFT is an excellent tool for materials, interface and surface modelling. Basically, it establishes a most natural link between primary quantum mechanics and materials science. Now a days, there is huge list of standard software like VASP, Quantum ATK, Quantum Espresso etc., which has increased the popularity and easiness using DFT. The as mentioned DFT software's are developed and tested by an international community of the theoretical researchers around the world. A huge DFT community all around the world is also responsible for the fast prototyping, improving and approval of new advances in the various field. It is also noted that DFT is not free of shortcomings, and it is not work for every material or every property. For the example: the vdW Waals binding in materials is not described previously, now Grimme-1 and 2 are used to incorporate those corrections. optical absorption spectra are red-shifted, and the PBE functionals underestimate the bandgap calculations, therefore hybrid -DFT functionals are used to correct the error. In this thesis, we are using Quantum-ATK software from Synopsys (Atomistic Simulation Software | Quantum ATK - Synopsys) for our work.

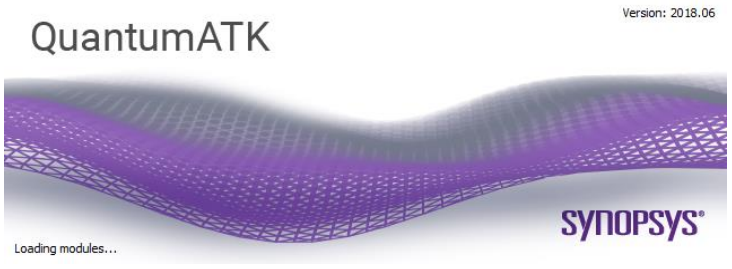

1.6 Physical Properties of $MoSe_2$

$MoSe_2$ is an atomically thin 2D materials with a direct band gap of 1.5 eV [25-27]. The natural phase bulk $MoSe_2$ has Mo atoms in trigonal prismatic coordination with Se atoms, and the layers are stacked in various order held together by van der Waals forces [26, 28, 29]. In 2L-$MoSe_2$, the space group: $P6_3/mmc$ is 2R and the space group: $R3m$ 3R matches is 3R phases, matches to the AB- and AB stacking [29-32]. The 3R phase has the broken inversion symmetry, whereas, in the 2H phase, the net inversion symmetry depends on whether there is an odd or even number of layers [33]. Fig. 1.6 shows the co-ordination structure and crystal structure of monolayer $MoSe_2$, where 'Mo' and 'Se' atoms form a 2D hexagonal lattice with trigonal prismatic coordination. A few important physical properties of monolayer MoS_2 are summarized in Table 1.1.

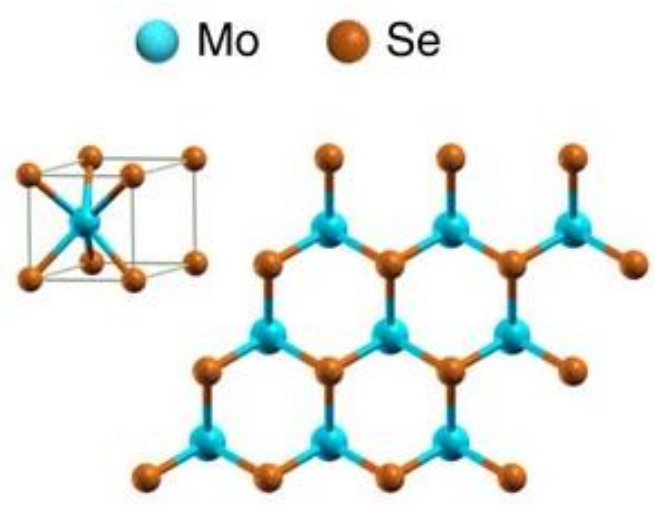

Fig 1.6: Coordination structure and crystal structure of monolayer $MoSe_2$ **[34].**

Table.1 Structural, chemical and electronic properties of $MoSe_2$ monolayer

Material	**Molar Mass(gm/mol)**	**Appearance**	**Density (g/cm^3)**	**Lattice Parameter(Å)**	**Melting Point(k)**	**Energy Gap(eV)**	**Electron concentration (Cm^{-3})**
MoSe2	253.86	Crystalline Solid	6.90	a = 3.288 c = 12.92 (for monolayer) a = 3.288 c = 15 (for bilayer)	1473	1.60 (direct, Monolayer), 1.25 (indirect, Bilayer), 0.95 (indirect, Bulk)	0.35-1.6·1017 (single crystal)

1.7 Motivation of the Work

In recent days, the TMDC materials have received a notable amount of interest due to their attractive electronic and optoelectronic properties and adaptable potential applications in next-generation 2D electronics. TMDCs monolayers are the atomically thin semiconductors (MoS_2, WS_2, $MoSe_2$…etc.) with excellent optical and electrical properties[1, 25, 35]; much effects going on the fabrication of 1L-TMDCs based electronic devices for various applications [36-38]. All the 1L-TMDCs based devices face critical issues such as high contact resistance and lack of suitable doping methods [36, 38-40]. However, as compare to monolayer, the bilayer TMDCs are particularly attractive for applications in Field Effect Transistors (FETs) [31, 41, 42], logic devices [40], and sensors [43]. Till now, most of the work, reported on MoS_2, WS_2 and WSe_2, however very few works reported on $MoSe_2$, this is also may be due to unmature growth and synthesis process of $MoSe_2$ materials as compare to MoS_2 and WS_2.Strain engineering in TMDCs materials is particularly exciting due to their ability to withstand extreme mechanical deformations before rupture [20-23]. It can be practically induced in TMDCs via mechanically stretching, bending, and clamping to the substrates [24]. Several experimental [25, 26] and theoretical studies [27, 28] reported the effect of strain on the band structure of 1L-TMDCs. However, reports on the effect of strain on the electronic structure of 2L-TMDCs, particularly with different stacking order, are scarce. It is of both fundamental and practical interest to know the similarities and evolution of the band structures under various imposed strain conditions.

Similarly, external E-field play a very vital role in present day electronics, it effects on variation of bilayer TMDC materials with different stacking order is very important.

Therefore, the purpose of this thesis work is to present a detailed study of the role of biaxial strain and external E-Field on the electronic structure of 2L-$MoSe_2$ of AB and AA stacking order.

CHAPTER-2

Literature Review

Due to the various additional degree of freedom, the bilayer-TMDC materials have been explored, as compared to free-standing monolayer. Here, we have presented literature review from last 6 years regarding recent work on bilayer TMDCs materials and effect of strain and electric field on the electronic and Optical properties.

In 2013, Conley, H.J., et al. [44] demonstrated "*Bandgap Engineering of Strained Monolayer and Bilayer MoS_2*" reported that strain-caused phonon softening, band gap modulation, and a transition from an optically direct to an optically indirect material in strained MoS_2 samples.

In 2014, Zhuang, H.L. and R.G. Hennig [45] demonstrated "*Tunable Electric Properties of Bilayer α-GeTe with Different Interlayer Distances and External Electric Fields*" reported van der Waals (vdW) bilayer α-GeTe has an indirect band structure with the bandgap value of 0.610 eV and α-GeTe has similarly attractive efficient light harvesting.

In 2014, He, J., K. Hummer, and C. Franchini [33] demonstrated "*Stacking effects on the electronic and optical properties of bilayer transition metal dichalcogenides MoS_2, $MoSe_2$, WS_2, and WSe_2*" reported distinct crystal structure and physical properties in TMDCs with different stacking orders.

In 2016, Hu, X., L. Kou, and L. Sun [46] reported "*Stacking orders induced direct band gap in bilayer $MoSe_2$-WSe_2 lateral heterostructures*" reported that direct band gap can be in hetero bilayer $MoSe_2$-WSe_2 heterostructure through alternating stacking orders.

In 2017, Ma, Y., et al. [47] reported **"***Effect of an external electric field on the electronic properties of SnS_2/PbI_2 van der Waals heterostructures*" reported a van dar waal heterostructure of SnS_2 and PbI_2 features well behaved electronics property under implemented external electric field. The external Electric field not only influences the band structure which modifies from semiconductor

to metal but also forces on band alignment that experiences a conversion between type-I straddling-band alignment type-II broken-gap, resulting to a different spatial distribution of the lowest energy electrons and holes.

In 2018, Cortés, N., et al. [48] reported "*Stacking change in MoS_2 bilayers induced by interstitial Mo impurities*" concludes that AB'-stacked configuration is most stable with energy gain on top of the van der Waals interaction as a result of the Mo impurity levels powerfully hybridize with the closest atoms. Also, the stacking between TMDC bilayers throughout the growth process, their electronic properties are finely -tuned.

In 2018, Deng, S., L. Li, and M. Li [49] demonstrated "*Stability of direct band gap under mechanical strains for monolayer MoS_2, $MoSe_2$, WS_2 and WSe_2*" reported that the Young's modulus and band gap of these four materials display a pattern of $Y_{WS2}>Y_{MoS2}>Y_{WSe2}>Y_{MoSe2}$ and Eg-WS_2>Eg-MoS_2>Eg-WSe_2>Eg-$MoSe_2$. Therefore, they concluded that "softer" monolayer TX_2 have wider direct band gap areas and higher band gap, that is an essential characteristic for photoluminescence applications.

In 2019, Zhang, X., et al. [30] demonstrated "*Transition metal dichalcogenides bilayer single crystals by reverse-flow chemical vapor epitaxy*" reported remarkable improved electrical characteristics of 2L- $MoSe_2$ FET with AA stacking order as compared to 2L AB-stacking was observed.

In 2019, Xiao, X.-B., et al [50] demonstrated **"**Electric Field Controlled Indirect-Direct-Indirect Band Gap Transition in Monolayer InSe" reported in monolayer InSe Indirect-direct-indirect band gap transition is observed when the electric field strength is increased continuously. Therefore, the global band gap is reduced gradually to zero, indicating that semiconductor-metal transformation happens.

In 2020, Peng, G., et al. [31] demonstrated " *controllable epitaxial growth of $MoSe_2$ bilayers with different stacking orders by reverse-flow chemical vapor deposition*". In this paper author reported stacking order plays an important role in electronic and optical properties of 2D TMDC materials.

Also, using the chemical vapor deposition (CVD) technique, the synthesis of high-quality and large area 2L-TMDCs crystals with various stacking orders is observed.

In 2020, Somvanshi, *et al.* [51] demonstrated "*Improved current density and contact resistance in bilayer $MoSe_2$ field effect transistors by AlOx capping*" author reported that advanced current density, with high mobility in $MoSe_2$ bilayer FETs as compare to monolayer MoSe2 based FETs.

In 2020, Guo, J., et al. [52] demonstrated *Strain Engineering on the Electronic and Optical Properties of WSSe Bilayer*" in this paper reported that by comparing the binding energies of various stacking order, the most favorable stacking of the WSSe bilayer is observed.

In 2020, Peng, Z., et al. [53] demonstrated "*Strain engineering of 2D semiconductors and graphene: from strain fields to band-structure tuning and photonic applications*" author reported large quantity of advances in the application of strain in 2D materials (especially TMDCs and graphene) to alter and manipulate their unique optical properties.

In 2020, Chaves, A., et al. [10] demonstrated "*Bandgap engineering of two-dimensional semiconductor materials*" reported the significance of 2D semiconductors gives a new platform to explore band structure engineering effects.

In 2020, Postorino, S., et al. [54] demonstrated *"Strain-induced effects on the electronic properties of 2D materials*" reported the impact of uniform biaxial compressive and tensile strain on the electronic properties of several 2D materials starting from semi metallic ones, just like the X-enes, to semiconductors like nitrides and TMDCs.

In 2022, Ghosh, S.K. and D. Somvanshi [55] demonstrated "*First-principal insight of the gold-metal interaction to bilayer $MoSe_2$ of AB and AA stacking order*" reported due to significantly increased carrier injection and higher orbital overlap, the Au/ 2L-AA $MoSe_2$ performed as a better than Au/2L-AB $MoSe_2$.

Chapter 3

Electronic Structure of Monolayer $MoSe_2$, and Bilayer $MoSe_2$

3.1 Monolayer $MoSe_2$:

Monolayer MoSe2 is an important member of TMDC semiconductor family. Here, in this chapter first, we optimized the monolayer $MoSe_2$ unit cell and analyze the bandstructure, Projected Density of State (PDOS), Effective Mass, Total Energy and optical spectrum. The optimized lattice parameters of the $MoSe_2$ are a = b = 3.34813 Å and c = 13.1593 Å, with the bond length (d_{Mo-Se}) of 1.70131 Å, which is very close to the experimentally reported values. [56] . We have taken a supercell size of 3×3×1, in this work. The total number of atoms in monolayer $MoSe_2$ = 27. The schematic diagram of monolayer MoSe2 is shown in Fig. 3.1.

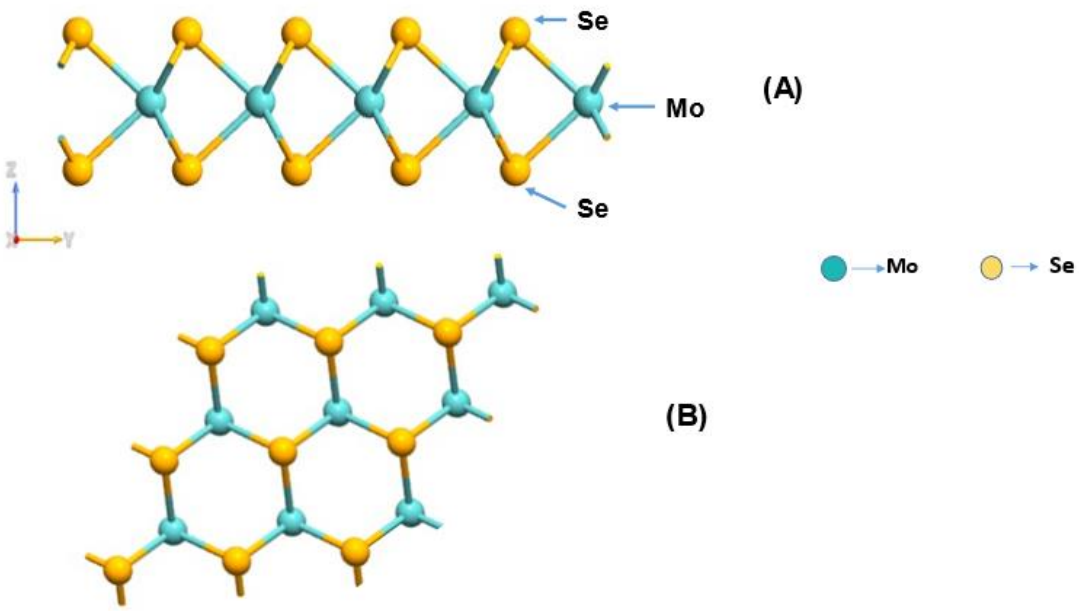

Fig 3.1: Schematic atomic structure of monolayer $MoSe_2$ (a) Side view (b) Top view

3.2 Bilayer $MoSe_2$ of AB and AA stacking order:

Now, further we have optimized the $MoSe_2$ bilayer unit cell with AB and AA stacking order and analyze the bandstructure, projected Density of State (PDOS), effective Mass, total Energy and optical Spectrum. Here, first we have taken a $MoSe_2$ bilayer of AB stacking order and optimized it. The optimized lattice parameters of the $MoSe_2$ are a = b = 3.347703 Å and c = 20 Å, with interlayer distance (for Se) = 3.07 Å & (for Mo) = 6.42707 Å, which is very close to the experimentally reported values [57]. We have got the indirect bandgap value of 1.09 eV which is very close to reported values [58]. Here, total number of atoms in bilayer $MoSe_2$ = 54. The schematic diagram of AB stacked bilayer MoSe2 is shown in Fig. 3.2 with top and side view.

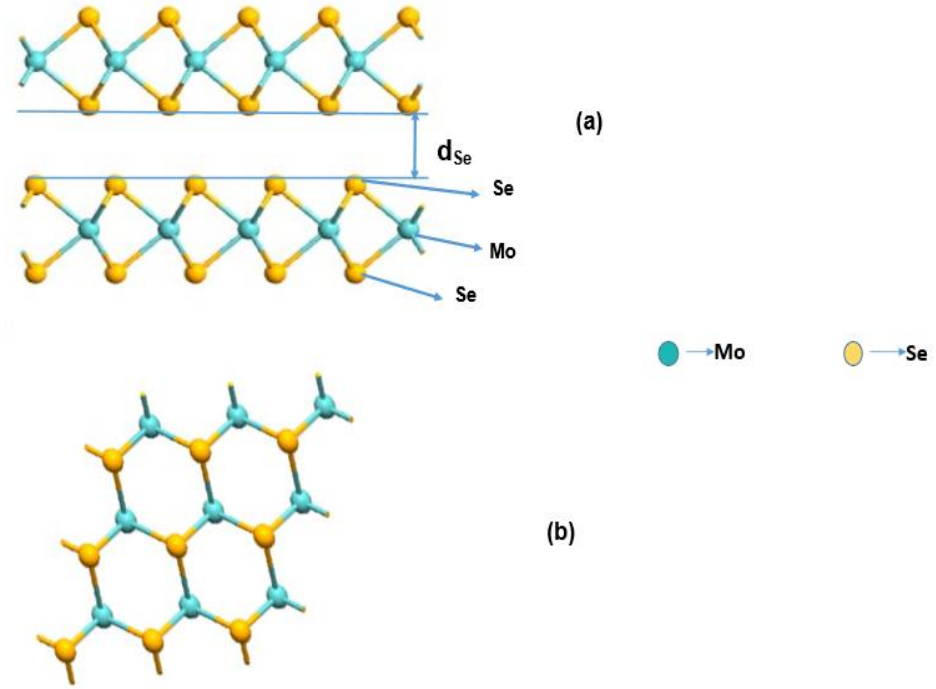

Fig 3.2: Schematic atomic structure of bilayer AB Stacking $MoSe_2$ (a) Side view (b) Top view

Now further, we have optimized the $MoSe_2$ bilayer unit cell with AA Stacking order and analyze the band structure, projected Density of State (PDOS), effective Mass, total energy and optical Spectrum. Here, we have taken a $MoSe_2$ bilayer with AA stacking order and optimized it. The optimized lattice parameters of the MoSe2 are a = b = 3.346695 Å and c = 20 Å, with interlayer distance (for Se) = 3.67 Å & (for Mo) = 6.42707 Å, which is very close to the experimentally reported values. We have got the indirect bandgap value of 1.25 eV which is very close to reported

values [59]. Here, Total number of atoms in bilayer $MoSe_2$ = 54. The schematic diagram of AA stacked bilayer MoSe2 is shown in Fig. 3.3.

It is clear that as compare to AA stacked bilayer $MoSe_2$, AB stacked bilayer $MoSe_2$ show stronger interlayer coupling, shorter interlayer distance. It is due to in AA stacking, each Se atom of the upper layer sits on top of the same Se atom belonging to the lower layer. It leads to large repulsions between electrons belonging to the Se atoms, which increasing interlayer distance [29, 30]. Opposite behaviour observed in case AB stacked MoSe2. Due to the smaller interlayer distance stronger electronic and mechanical coupling strength is observed in AB stacked Bilayer $MoSe_2$ [60].

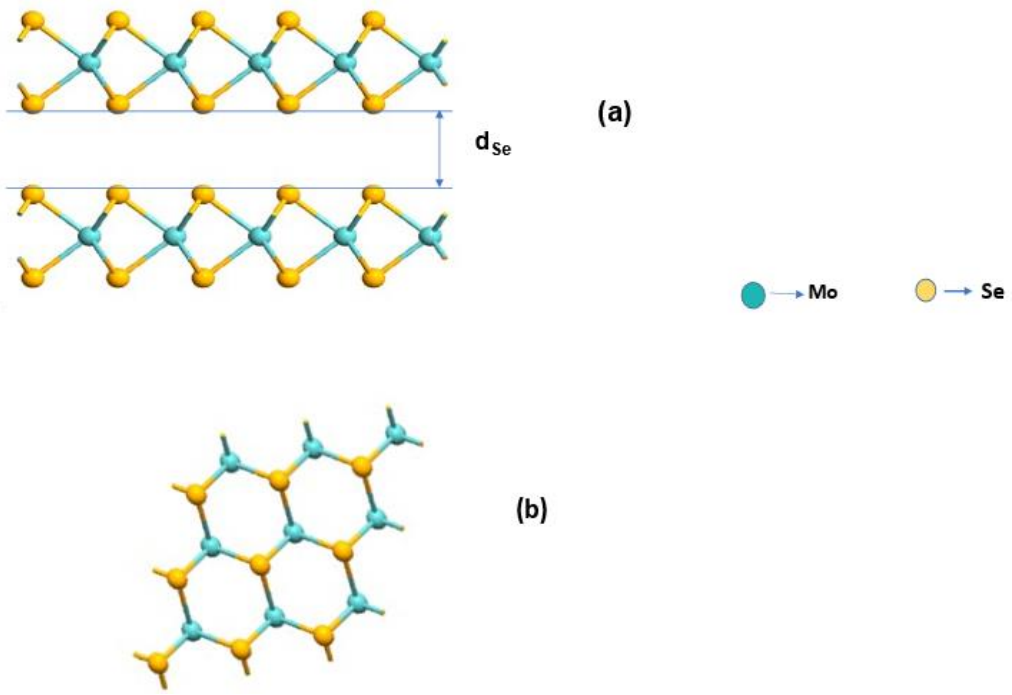

Fig 3.3: Schematic atomic structure of bilayer AA Stacking $MoSe_2$ (a) Side view (b) Top view

3.3 Electronics and Optical characterization:

A) Geometry Optimization (Computational Method)

The modeling of monolayer $MoSe_2$ and Bilayer $MoSe_2$ of AB and AA stacking structures are based on Quantum Atomistix Tool Kit simulation tools. The exchange-correlation functionals were

described using generalized gradient approximation (GGA) in the Perdew–Burke–Ernzerhof (PBE) form [61].

In LCAO (linear combination of atomic orbitals), we have taken broadening as 300K with density mesh cutoff as 125 Hartree and the k-point sampling of 5×5×1(for both monolayer and bilayer) to optimize all the structures. We have chosen Grimme DFT-D2 Van der waals correction. The bilayer structures are fully optimized to minimize total energy of the system with the force and tolerance limit on each atom is less than 0.01 eV/Å and 10^{-5}. We have taken Stress error tolerance as 0.001eV/Å3. We have chosen fix Bravais lattice type lattice constraints. A vacuum space of 20Å is included avoid the coupling between neighboring cells. In PAW, we have taken broadening as 300K with wave function cutoff as 23.88 Hartree and the k-point sampling of 5×5×1(for both monolayer and bilayer) to optimize all the structures. We have chosen Grimme DFT-D2 Van der waals correction. We have chosen projected augmented wave (PAW) pseudopotential method.

B) Band structure

Band structures are an allowed electronic energy levels of a material system and the bandgap is basically energy range in a material where no electron can exit. It is defined as energy difference between the valance band maximum (VBM) the conduction band minimum (CBM) along the symmetry line along Brillouin zone. By seeing band structure plot, we can identify whether a material is metallic, or insulating, or it is direct/indirect band gap materials. The curvature of the bands can reflect the carrier mobility through those bands

C) Projected DOS

The Projected Density Of States (PDOS) is used to shows the involvement of different orbitals to the DOS. It can be written as

$$\mathbf{D}(\epsilon) = \sum_n \boldsymbol{\delta}(\epsilon - \epsilon_n)$$

where n contains all the quantum numbers of the system.

Now the PDOS associated to a given projection direction M is defined as

$$\mathbf{D_M}(\epsilon) = \sum_n \boldsymbol{\delta}(\epsilon - \epsilon_n) \langle \psi_n | \hat{P}_M | \psi_n \rangle$$

ψ_n are the eigenstates and $\hat{P}_M$ is a projection operator.

D) Effective Mass

The effective mass of a semiconductor is determined by fitting the E-k diagram around the conduction band minimum (CBM) or the valence band maximum (VBM) by a parabola. The effective mass of electrons and holes is related to the local curvature of the electronic band energy, E(k):

$$m_{eff} \propto \frac{1}{\frac{\partial 2E(K)}{\partial K2}}$$

E) Total Energy

In ATK-DFT, the total energy object returns the free energy given by

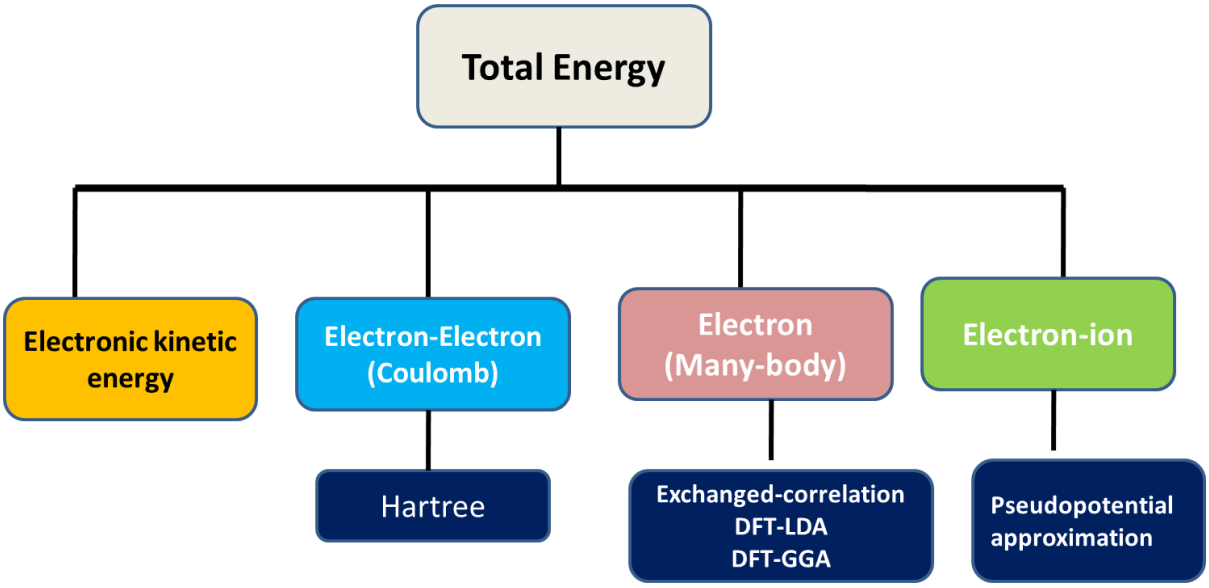

Fig. 3.4 shows the different contribution of energy in total energy in DFT calculations.

F) Optical Spectra

The monolayer $MoSe_2$ and bilayer $MoSe_2$ with AB and AA stacking order models are simulated to determine the optical properties, which is determined by the imaginary part of the frequency-dependent complex dielectric function $\varepsilon(\omega) = \varepsilon_1(\omega) + \varepsilon_2(\omega)$ is calculated. The energy-

dependent absorption coefficient α (ω) can be deduced from ε_1 and ε_2 and mathematically written as

$$\alpha\ (\omega)\ = \sqrt{2}\omega\ [\sqrt{(\varepsilon_1^2(\omega)+\varepsilon_2^2(\omega))}-\varepsilon_1(\omega)]^{1/2} = \frac{2k\omega}{C}$$

where ω is the frequency of light, c is the velocity of light κ is the extinction coefficient. The imaginary part ε_2 (ω) is used to measure the optical absorption in materials and the real part ε_1 (ω) is associated with dispersion in materials deduced from the imaginary part ε_2 by the well-known Kramer−Kronig relation.

3.4 Result and discussion

3.4.1 Monolayer $MoSe_2$

(a) Geometry optimization: -

To optimized the k-point sampling to find the ground state energy for MoSe2 monolayer we vary the k-Mesh from 2×2×1 to 9×9×1 and calculated total energy for each k-point. Fig. 3.4 shows the plot of total energy versus k-point for monolayer MoSe2. From Fig 3.4. we can see that for the monolayer $MoSe_2$ the ground state energy is found at 5×5×1 sampling k-point. This means the structure is most stable at 5×5×1 sampling k-point.

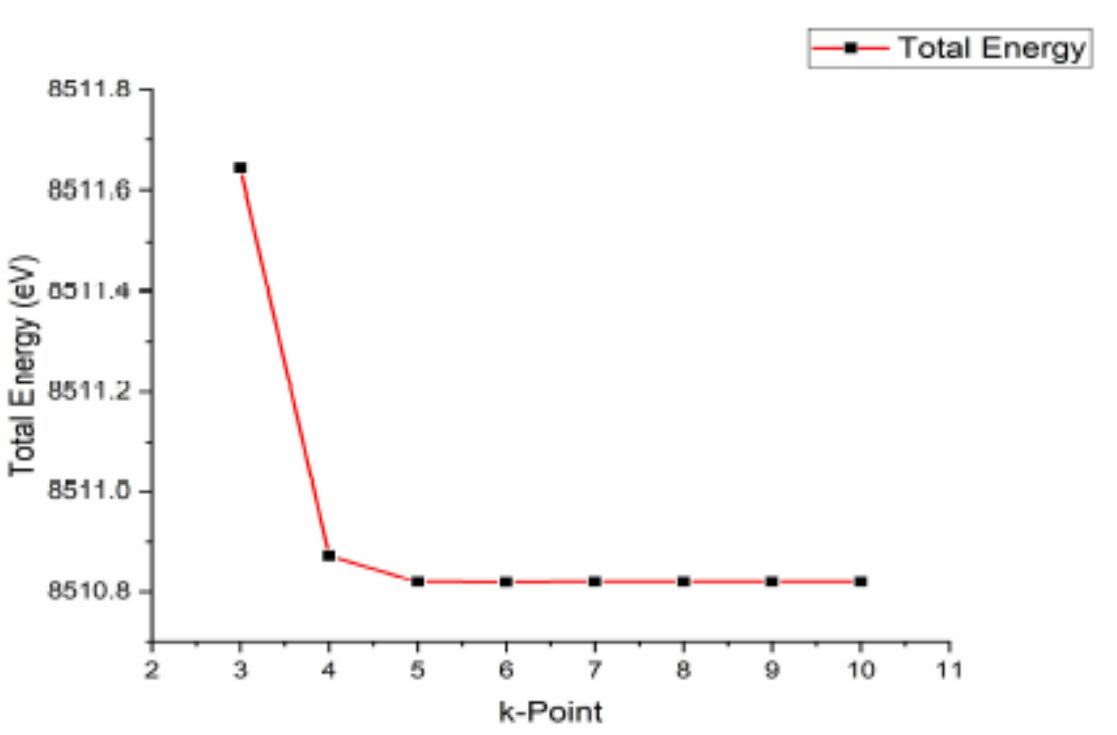

Fig. 3.5 Optimization of Mono-Layer MoSe2

(b) Band structure and Projected DOS: -

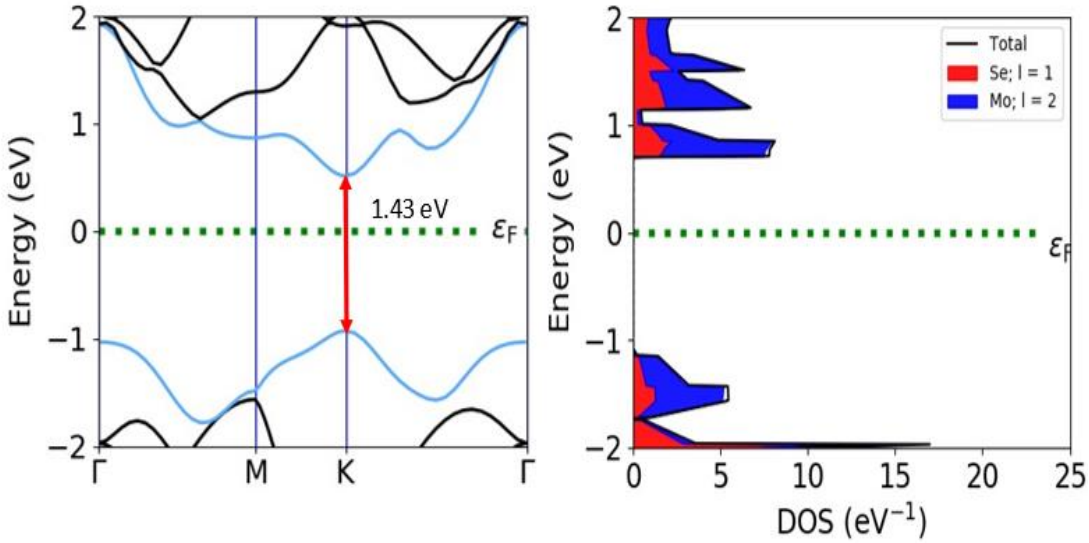

Fig 3.6: Direct bandgap in Band structure and Projected DOS of Mono-layer of MoSe2

Here we can see from bandstructure that 1-L $MoSe_2$ shows direct band-gap of 1.43eV. Both the valence band maxima (VBM) and the conduction band minima (CBM) occur at the K point,

indicating that the bandgap is of direct type. From PDOS, it is clear that p-orbital of Se atom and d -orbital of Mo atoms are main contributor in the PDOS of MoSe2.

(c) Effective Mass: -

Effective mass of Mono-layer $MoSe_2$ for electron,

$$m_e^* = 0.605\ m_0$$

Effective mass of Mono-layer $MoSe_2$ for hole,

$$m_h^* = 0.710\ m_0$$

where, m_0= Free electron mass = $9.11 * 10^{-31}$ Kg

(d) **Optical Spectrum:** - The optical spectrum shows the main absorption in UV and visible region for Mono-layer MoSe2. In 1-L MoSe2, light absorption ability is efficient because of direct bandgap.

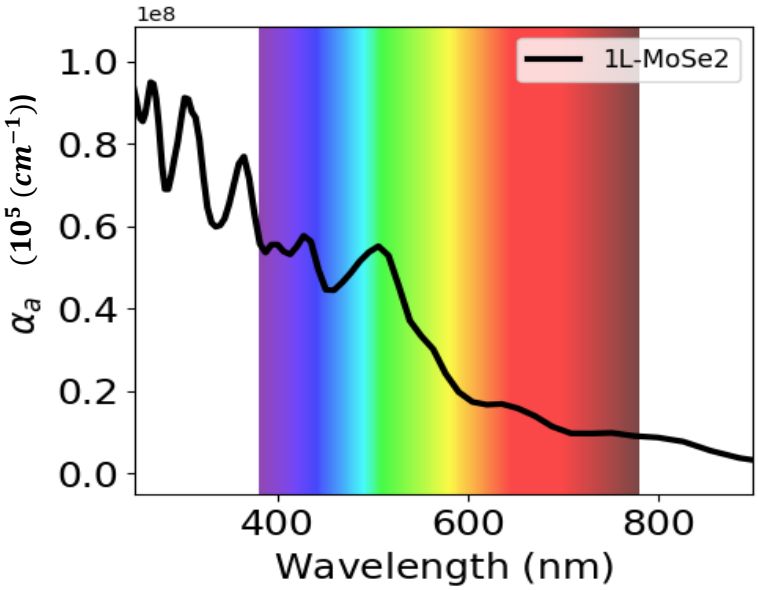

Fig 3.7: Optical Spectra of Mono-layer $MoSe_2$

(e) Total Energy: -

Total Energy = -8511.57 eV

3.4.2 Bilayer $MoSe_2$ of AB and AA stacking order

Similar to MoSe2, we have determined the ground state energy of 2-L $MoSe_2$ of AB and AA MoSe2, with varying the k-Point sampling from 3×3×2 to 10×10×2. From Fig. 3.7 we can see that for the 2-L $MoSe_2$ the ground state energy is found at 5×5×2 sampling k-point. This means the structure is most stable at 5×5×2 sampling k- point.

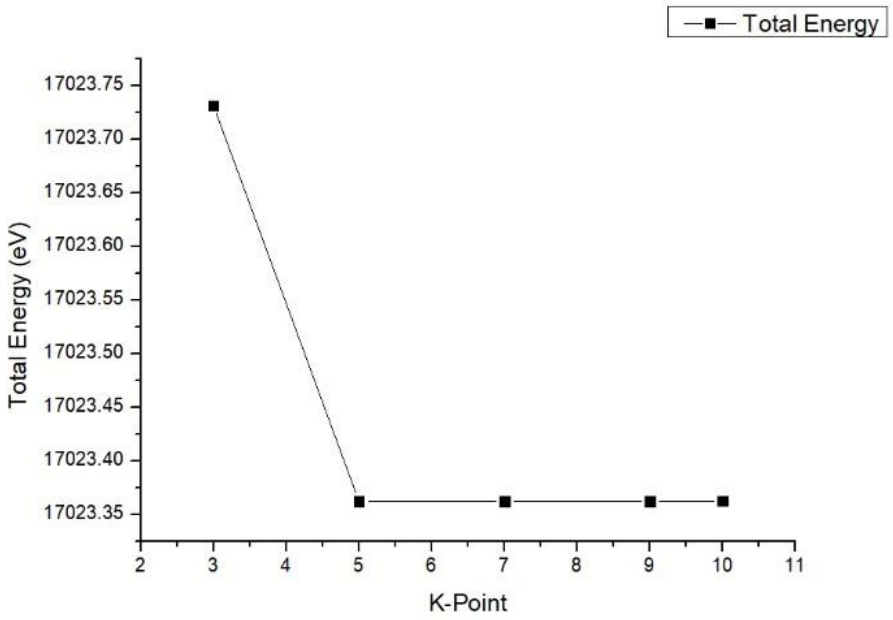

Fig 3.8 Optimization of k-point sampling for Bi-layer $MoSe_2$

A. AB Stacking $MoSe_2$ bilayer

a) Band structure and Projected DOS:

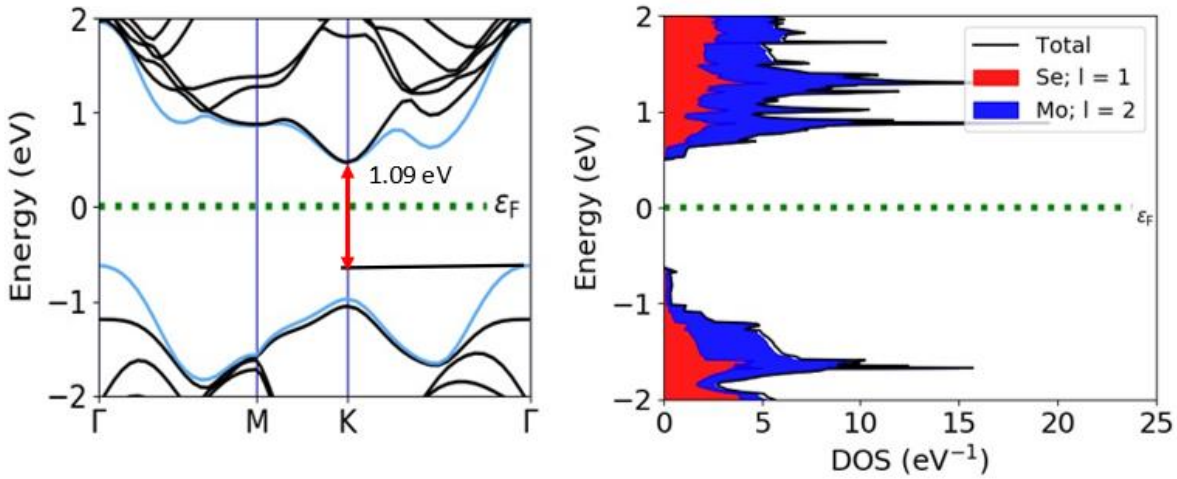

Fig 3.9: Indirect bandgap in band structure and Projected Density of State (PDOS) of Bi-layer $MoSe_2$ with AB stacking order

b) Effective Mass: -

Effective mass of AB stacking Bi-layer $MoSe_2$ for electron,

$$m_e^* = 0.528\ m_0$$

Effective mass of AB stacking Bi-layer $MoSe_2$ for hole,

$$m_h^* = 1.307\ m_0$$

where, m_0= Free electron mass = $9.11 * 10^{-31}$ Kg

c) Optical Spectrum: -The optical spectrum shows the main absorption in UV and visible region for Bi-layer $MoSe_2$ of AB stacking order. In Bi-layer $MoSe_2$, light absorption is less efficient than 1-L because of indirect bandgap type.

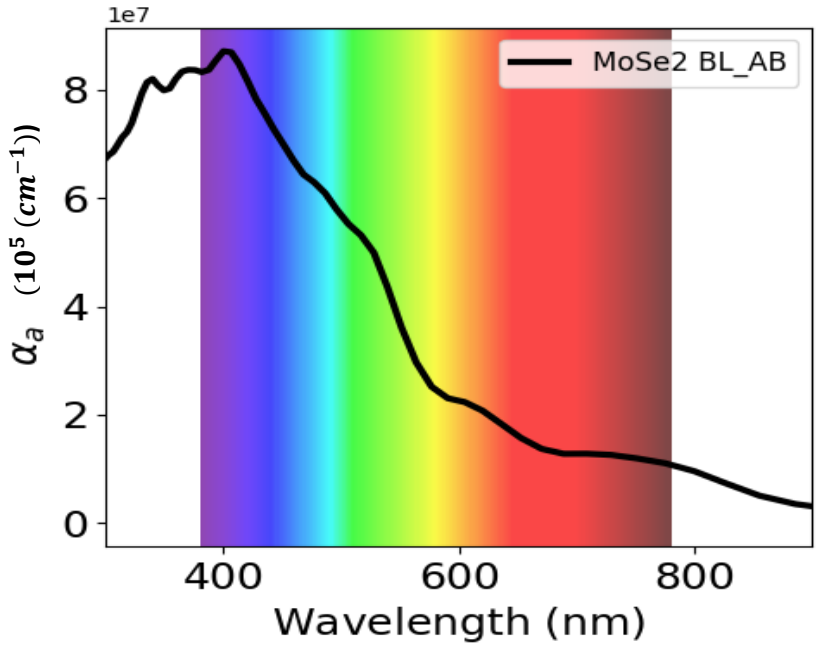

Fig 3.10: Optical spectrum of AB Stacking Bi-layer $MoSe_2$

d) Total Energy: -

Total Energy= -17023.45 eV

B. AA Stacking $MoSe_2$ bilayer

a) Band structure and Projected DOS: -

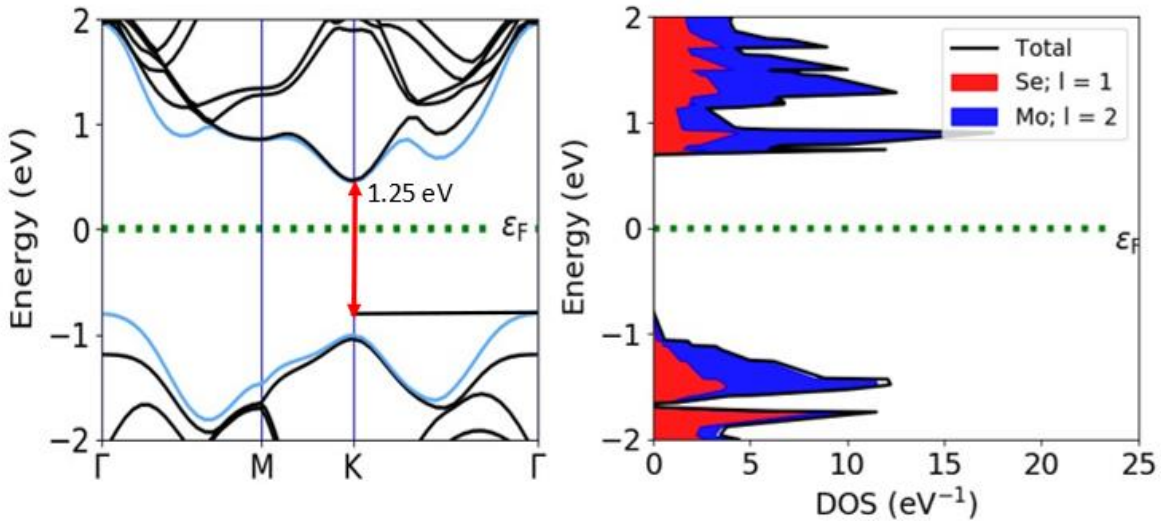

Fig 3.11: Band structure and PDOS of a Bi-layer $MoSe_2$ with AA Stacking order

b) Effective Mass:

Effective mass of AA stacking Bi-layer $MoSe_2$ for electron,

$$m_e^* = 0.590\ m_0$$

Effective mass of AA stacking Bi-layer $MoSe_2$ for hole,

$$m_{h^*} = 2.364\ m_0$$

where, m_0= Free electron mass = $9.11 * 10^{-31}$ Kg

c) **Optical Spectrum:** The optical spectrum shows the main absorption in UV and visible region for Bi-layer $MoSe_2$ of AA stacking order. In Bi-layer $MoSe_2$, light absorption is less efficient than 1-L because of indirect bandgap type.

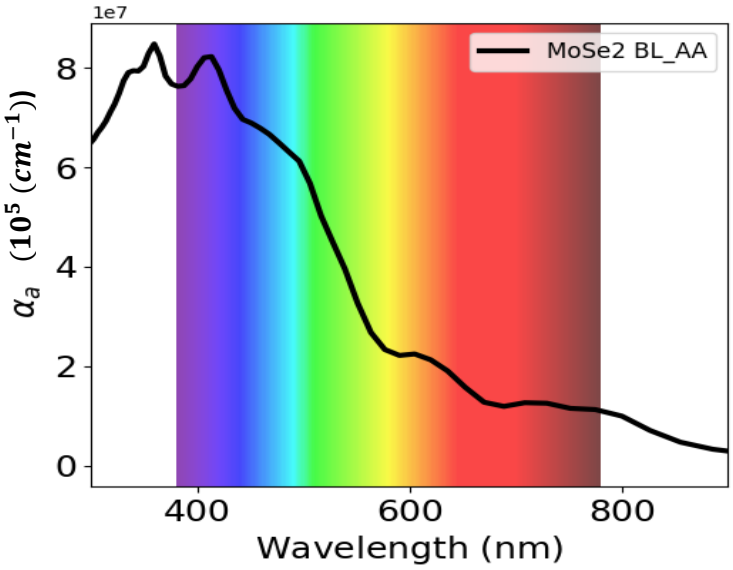

Fig 3.12: Optical spectrum of AA Stacking Bi-layer $MoSe_2$

d) Total Energy:

Total Energy= -17023.29 eV

Here we can see from band structure that Bi-layer $MoSe_2$ with AB stacking order shows indirect band-gap of 1.09eV and Bi-layer $MoSe_2$ with AA stacking order shows indirect band gap of 1.25eV. The valence band maxima (VBM) occur at T and the conduction band minima (CBM) occur at the K - point, indicating that the bandgap is of indirect type. From PDOS, we observed the contribution of p-orbital and d-orbital to the density of states for both AB and AA stacking Bi-layer $MoSe_2$.

The DFT-PAW method has its some advantages and disadvantages compared to the DFT-LCAO approach. Here, we analyzed band structure of AB stacked bi-layer $MoSe_2$ and AA stacked bilayer $MoSe_2$ using PAW calculator.

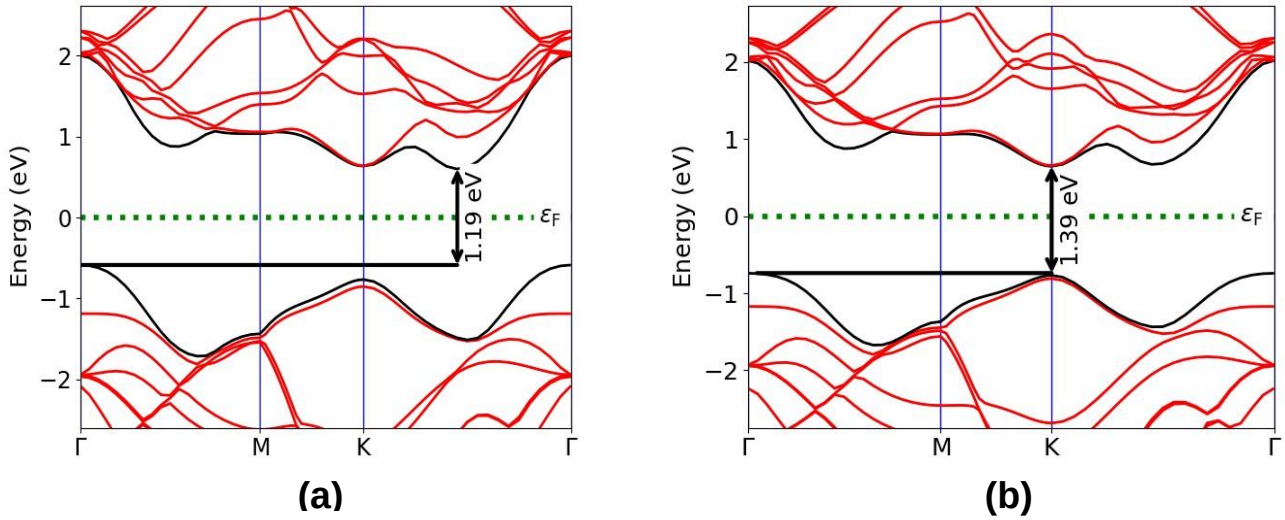

Fig 3.13: In PAW, bandstructure of (a) AB stacked Bi-layer $MoSe_2$, (b) AA stacked Bi-layer $MoSe_2$

Few parameters of the optimized structure such as lattice constant, band gap, Interlayer distance, total energy etc. are summarized in Table 3.1 [57, 59, 62].

Materials Parameters	Lattice constant (a) Å	Band gap (eV)	Interlayer distance (d_{Se}) Å	Band gap transition	Total energy (eV)
1L $MoSe_2$	3.348131	1.43	0	K->K (Direct)	-8511.57
2L-AB $MoSe_2$	3.347703	1.07	3.07	$T \rightarrow K$ (Indirect)	-17023.45
2L-AA $MoSe_2$	3.346695	1.30	3.67	$T \rightarrow K$ (Indirect)	-17023.29

Binding Energy:

Materials	**Upper layer Energy (eV)**	**Lower layer Energy (eV)**	**Total Energy (eV)**	**Binding Energy (eV)**
AB- stacked bilayer $MoSe_2$	-8511.57906	-8511.52282	-17023.35680	-0.2549
AA-stacked bilayer $MoSe_2$	-8511.57906	-8511.52245	-17023.24471	-0.14321

Binding Energy (E_B) is defined as total energy of a bilayer structure minus the sum of total energies of corresponding constituent monolayers. Here we observed that binding energy of AB stacking Bi-layer $MoSe_2$ (-0.2549 eV) ensures better energetic stability compared to that of AA stacking Bi-layer $MoSe_2$ (-0.1432 eV) [63].

Chapter 4

Effect of electric field on the electronic structure of bilayer $MoSe_2$ of AB and AA stacking order

The external electric fields have been applied to modify the electronic band structure of 2D materials. It has a great impact on the electronic structure of $MoSe_2$ bilayer with AB and AA stacking order which we have discussed in details [64].

In general, upon application of external transverse electric field in the positive (negative) z-direction (c-direction along the unit cell), the electron density increases (decreases) around the transition metal i.e., Mo atoms and increases/decreases around the two chalcogenides i.e., Se atoms. It is due to induction of a dipole moment along the direction of the electric field. Due to external E field, a potential difference also induces which causes splitting of energy bands belonging to different layers as well as shifting of the VBM and CBM [47, 65-67].

The schematic diagram of AB and AA stacked bilayer $MoSe_2$ under with metal electrode is shown in Fig. 4.1. In this work, we applied field along the z- direction in the range from −2.8 V/Å to +2.8 V/Å with an increment of 0.4 V/Å to AB and AA stacked bilayer $MoSe_2$.

4.1. AB Stacking bilayer $MoSe_2$

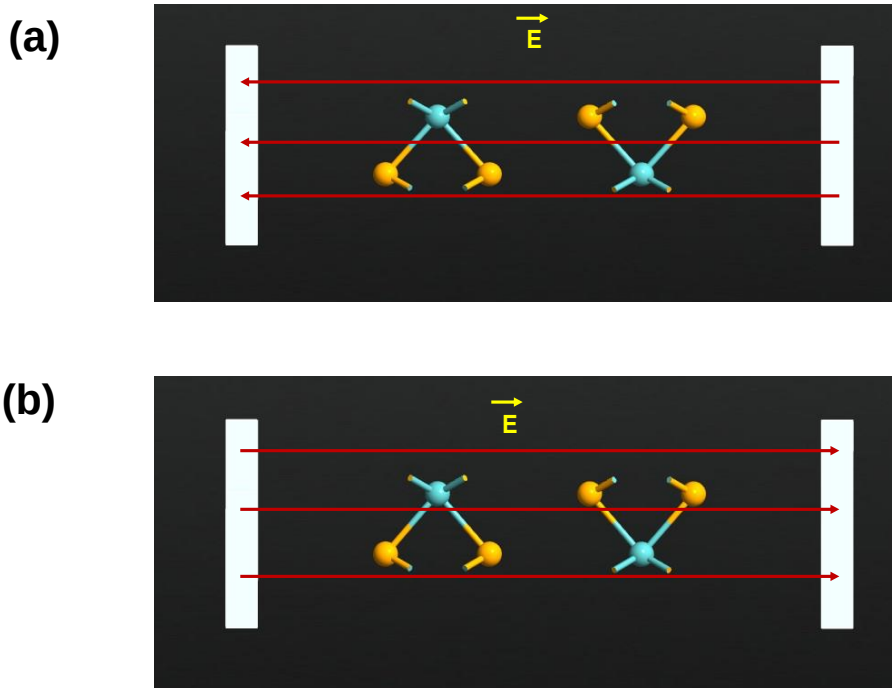

Fig 4.1: Schematic Diagram of 2L $MoSe_2$ AB Stacking with Electrodes (a) When we applied positive electric field, (b) When we applied negative electric field**.**

Table 4.1 summarizes the calculated band gaps and total energy for different values of transverse electric field for AB stacking bilayer $MoSe_2$ below.

Electric Field (V/Á)	Bandgap (eV)	Total Energy(eV)
-2.8	0	-17023.40390
-2.2	0.36	-17023.33757
-2	0.438	-17023.31907
-1.6	0.58	-17023.28745
-1.2	0.73	-17023.26292
-0.8	0.87	-17023.24544
-0.4	0.99	-17023.23496
0	1.09	-17023.35680
0.4	0.99	-17023.23496
0.8	0.87	-17023.24544
1.2	0.73	-17023.26292
1.6	0.58	-17023.28745
2	0.438	-17023.31908
2.2	0.36	-17023.33757
2.4	0.28	-17023.35787
2.8	0	-17023.40391

The value of bandgap and total energy calculated at each value of E-field as listed in Table. 4.1. The band structure of AB stacking $MoSe_2$ bilayer with different values of transverse electric field are shown in Fig. 4.3. Clearly, as we increase the value of + E- field, the band gap value decreases slowly and particular value of E, the band gap become zero and semiconductor to metal transition observed. As clearly visible in Fig. 4.2 (f).

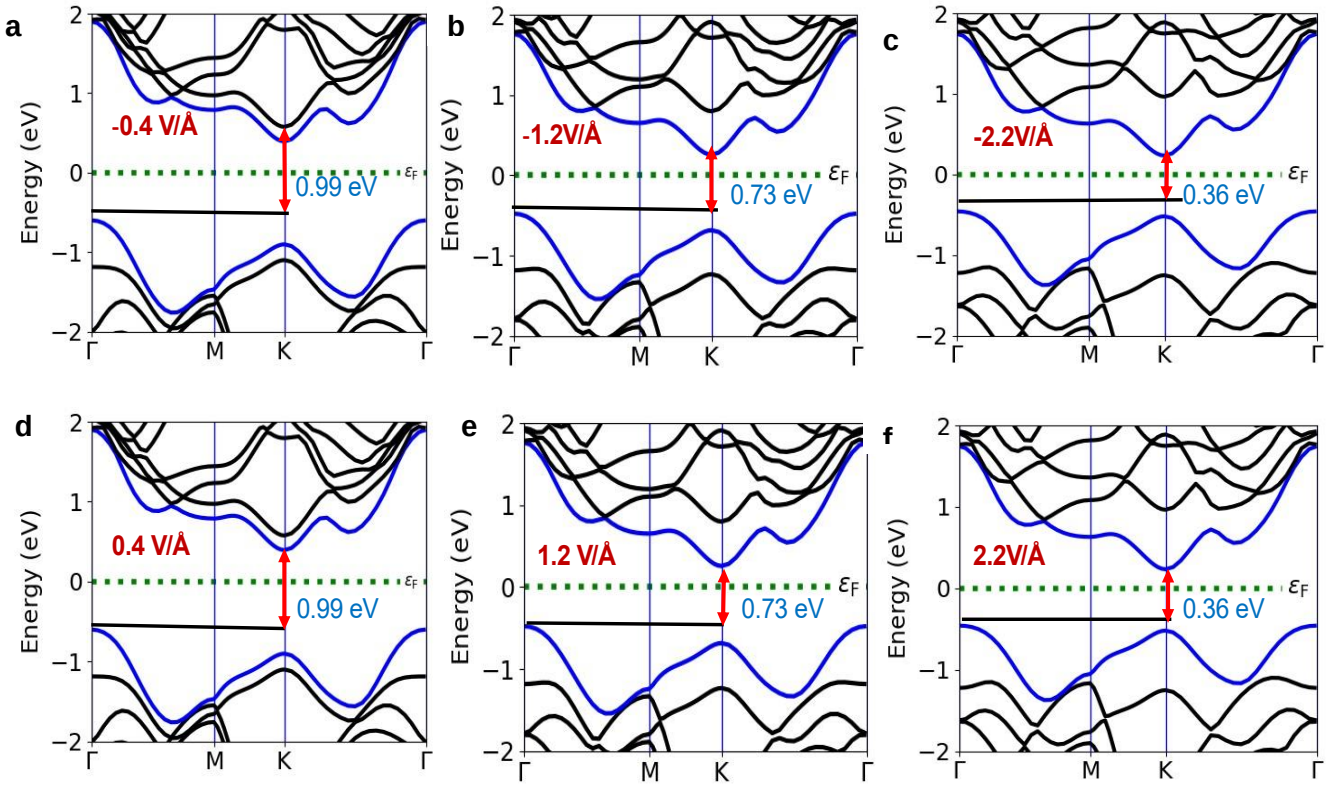

Fig 4.2: Band diagram of AB stacking $MoSe_2$ bi-layer with applied external Electric Field a)-0.4 V/Å, b) -1.2 V/Å, c) -2.2 V/Å, d) 0.4 V/Å, e) 1.2V/Å, d) 2.2 V/Å. The bandgap transition Γ-K and bandgap decreases from 1.09 eV to 0 eV as electric field increases from 0 V/Å to 2.8 V/Å

The band gap of AB stacking bilayer $MoSe_2$ decreases monotonically from the maximum (1.09 eV) at 0.0 V/Å to minimum (0 eV) at 2.8 V/Å in both, positive and negative direction along the z-axis. So, AB stacking bilayer $MoSe_2$ have been shown to have vastly different electronic behavior, ranging from semiconductor material to metallic material, when we applied external Electric field.

4.2 AA Stacking bi-layer $MoSe_2$

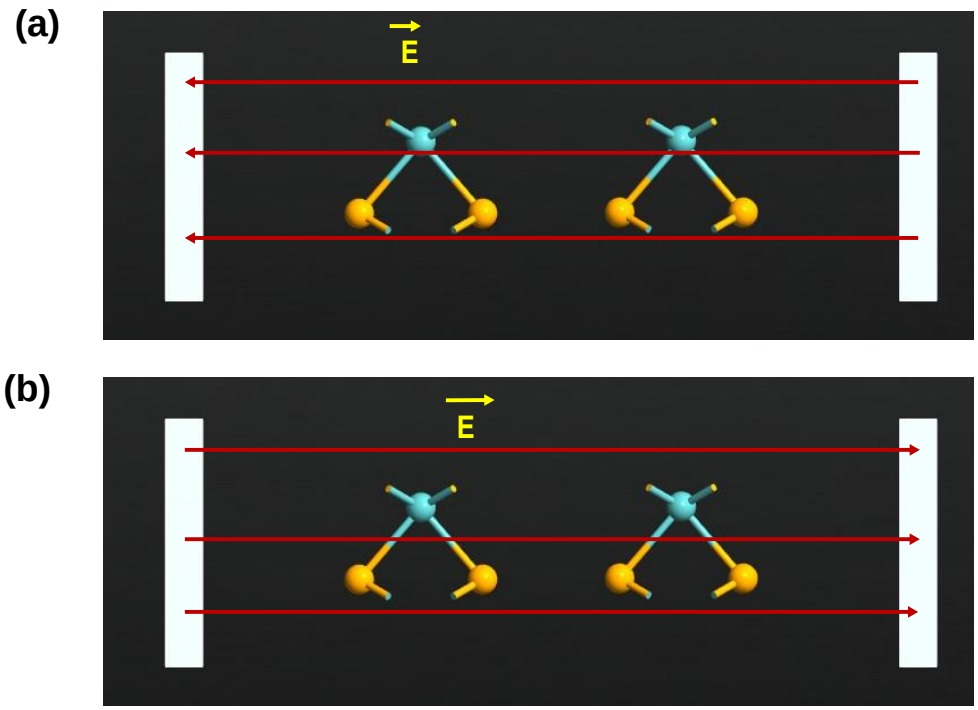

Fig 4.3: Schematic Diagram of 2L $MoSe_2$ AA Stacking with Electrodes (a) When we applied positive electric field, (b) When we applied negative electric field.

In the AA stacking MoSe2 bilayer, a transverse electric field along the z- direction in the range from −2.2 V/Å to +2.2 V/Å with an increment of 0.4 V/Å is applied. The band gap of AA stacking bilayer $MoSe_2$ decreases monotonically from the maximum (1.25 eV) at 0.0 V/Å to minimum (0 eV) at 2.2 V/Å in both, positive and negative direction along the z-axis. So, AA stacking bilayer $MoSe_2$ have been shown to have vastly different electronic behavior, ranging from semiconductor material to metallic material, when we applied external Electric field.

Table 4.2 summarizes the calculated band gaps and total energy for different values of transverse electric field for AA stacking bilayer $MoSe_2$.

Electric Field (V/Å)	Bandgap (eV)	Total Energy(eV)
-2.2	0	-17023.21185
-2	0.25	-17023.19550
-1.6	0.46	-17023.16762
-1.2	0.69	-17023.14605
-0.8	0.909	-17023.13069
-0.4	1.1	-17023.12150
0	1.25	-17023.24471
0.4	1.1	-17023.12149
0.8	0.91	-17023.13068
1.2	0.69	-17023.14604
1.6	0.46	-17023.16761
2	0.25	-17023.19548
2.2	0	-17023.21183

The band diagrams of AA stacking $MoSe_2$ bilayer with different values of transverse electric field are shown in Fig. 4.5.

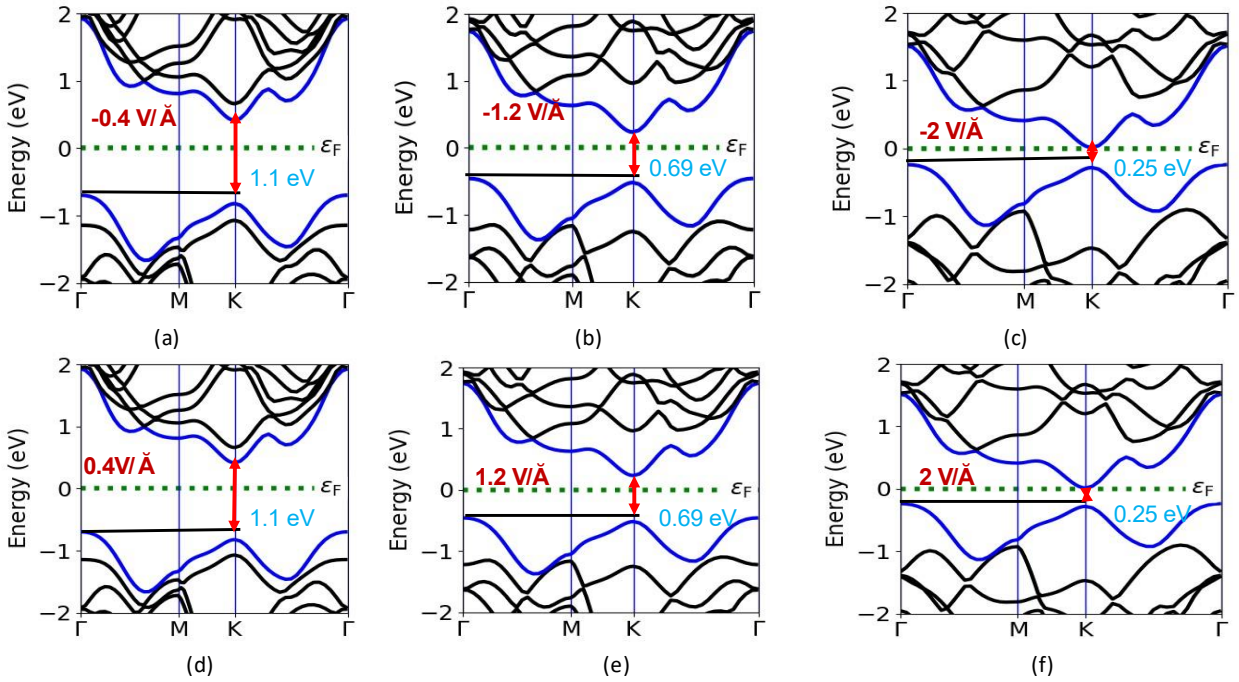

Fig 4.4: Band diagram of AA stacking $MoSe_2$ bi-layer with applied external Electric Field a)-0.4 V/Å, b) -1.2 V/Å, c) -2 V/Å, d) 0.4 V/Å, e) 1.2V/Å, d) 2 V/Å. The bandgap transition Γ-K and bandgap decreases from 1.25 eV to 0 eV as electric field increases from 0 V/Å to 2.2 V/Å

Fig. 4.5 compare the band gap values versus Electric field for both AB and AA stacked bilayer $MoSe_2$.

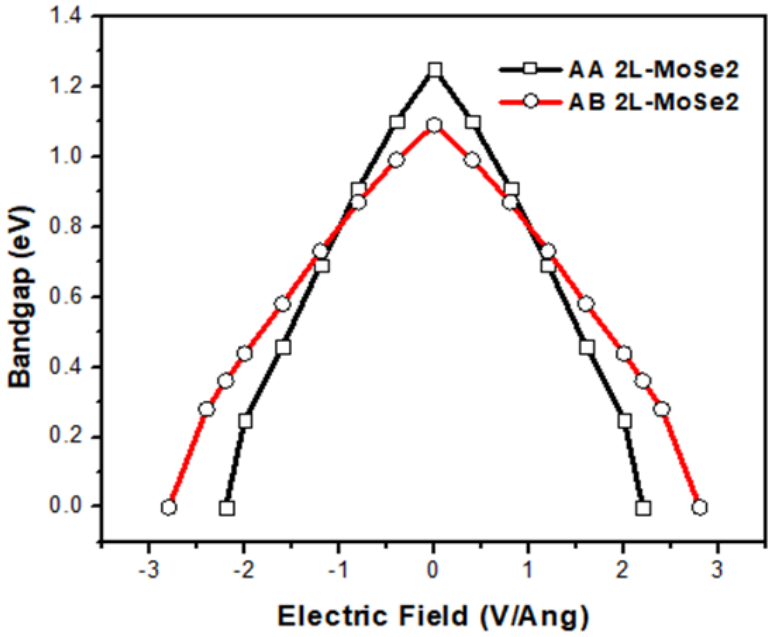

Fig. 4.5: Variation in Band gap of AB and AA stacking bilayer $MoSe_2$ with applied electric field.

Chapter 5

Effect of Biaxial strain on the electronic band structure of 2L $MoSe_2$ of AB and AA stacking order

As compare to traditional 3D bulk materials, the 2D materials have excellent mechanical flexibility. They can sustain a mechanical deformation on the order of 10-12 %. Therefore, they have excellent potential applications in the emerging areas such as flexibles electronic transparent display screen and wearable electronics. In contrast the 3D semiconductors can breakdown at strains only > 1% due to defects and dislocations

Strain engineering is an effective technique that changes the electronic structure and thus modulates various electronic and optical properties of 2D materials. Therefore, here, in this chapter we have applied a biaxial strain from -7 % to +7 %, where + and – signs represent tensile and compressive strain to analyzing its effect on bilayer $MoSe_2$ of AB and AA stacking order. We have applied the biaxial strain in the x and y direction to investigate the tunability of the electronic structure. It is noted that as compare to biaxial strain is the most effective compare to the uniaxial and shear strain [53, 54, 58, 65, 66, 68].

5.1 AB Stacking bilayer $MoSe_2$

First, we relax AB-stacked BL $MoSe_2$ at the PBE level, before studying the effects of ε on the electronic structure. The magnitude of biaxial strain can be defined by following relation $\varepsilon = (a_0 - a)/a \times 100\%$, where a_0 and a are the lattice constants of the strained and unstrained BL $MoSe_2$, respectively.

In general, upon application of biaxial strain, a reduction (enhancement) in interlayer distance is observed as strain varies from -7% to +7%. This is mainly due to the reduction (enhancement) in the coupling between the Mo and Se atoms during the tensile (compressive) strain (See Table 5.1). It is also observed that the total energy rises with tensile and compressive strain for AB-stacked $MoSe_2$ BL. All the lattice parameters, bond length, bandgap, total energy, and formation energy of AB-stacked $MoSe_2$ BL at strain varying from -7% to +7% have been shown in Table 5.1.

Strain(%)	Lattice Constant (Á)	Interlayer Distance(Á)	Bandgap(eV)	Bandgap transition	Total Energy(eV)
-7	3.08	3.22	0.94	K-> Σ_{min}	-157.88628
-6	3.11	3.21	1	K-> Σ_{min}	-158.13334
-5	3.15	3.20	1.066	K-> Σ_{min}	-158.33571
-4	3.18	3.15	1.12	K-> Σ_{min}	-158.49050
-3	3.21	3.166	1.18	K-> Σ_{min}	-158.61498
-2	3.251	3.18	1.24	K-> Σ_{min}	-158.70135
-1	3.284	3.195	1.22	T->Σ_{min}	-158.75128
0	3.317	3.214	1.185	T->K	-158.78518
1	3.35	3.21	1.04	T->K	-158.74702
2	3.38	3.144	0.826	T->K	-158.68532
3	3.41	3.148	0.66	T->K	-158.60274
4	3.45	3.124	0.5	T->K	-158.48671
5	3.48	3.16	0.385	T->K	-158.35120
6	3.516	3.099	0.23	T->K	-158.17565
7	3.55	3.095	0	-	-157.98319

Table 5.1: The relaxed lattice constants (a), Interlayer distance (d_{Se-Se}), the bandgap, and total energy (Etot)of the system under different compressive and tensile strain conditions.

To further analyze, we have plotted bandgap variations of both AB-$MoSe_2$ BL and AA-$MoSe_2$ BL with biaxial strain in one plot, as shown in Fig. 5.3. From the plot, we observed that the bandgap energy linearly decreases with tensile strain and when we applied 7% Strain, for AB stacking bilayer $MoSe_2$ have been shown semiconductor to metallic transition. However, we observed that it is increases to particular value of the compressive strain and further decreases to the higher value of compressive strain.

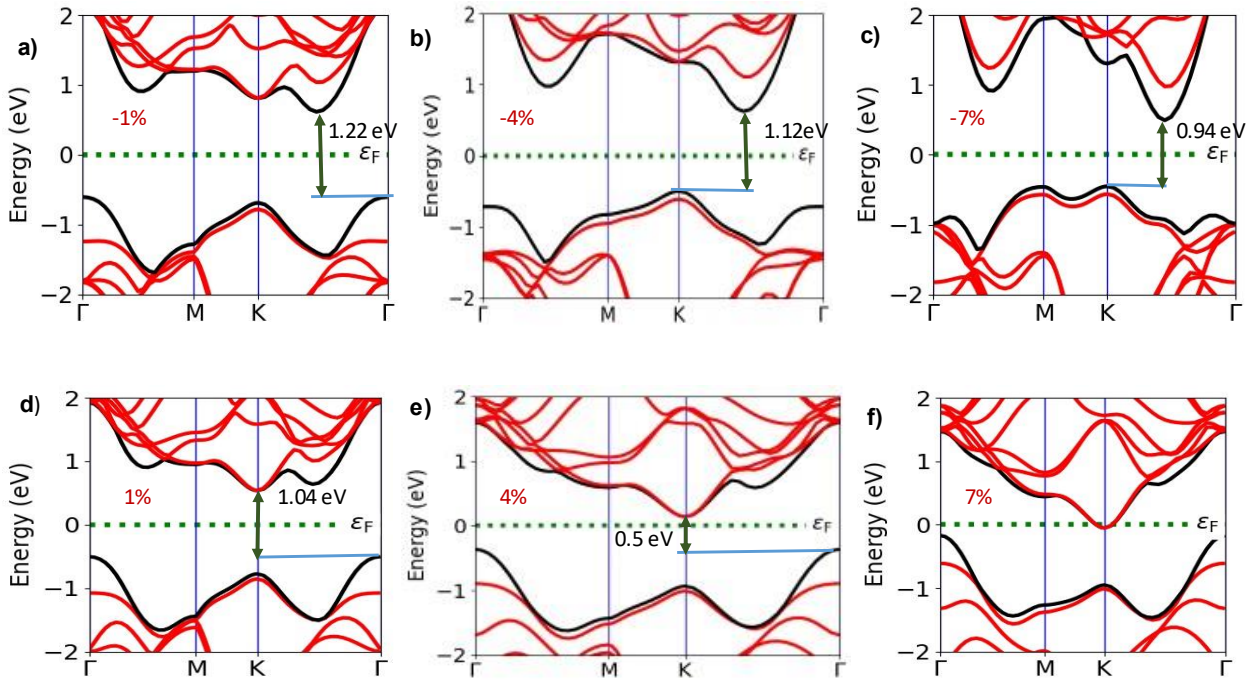

Fig 5.1: Band diagram of AB stacking $MoSe_2$ bilayer for biaxial compressive and tensile strain at ε = (a) -1%, (b) -4%, (c) -7%, (d) 1%, (e) 4% and (f) 7%. The bandgap transition changes K-Σ_{min} (-7% - -1.9%) to Γ-Σ_{min} (-1.8% - -1%) for compressive strain and Γ-Σ_{min} (0.01% - 0.04%) to Γ-K (0.05% - 6%) for tensile strain. The bandgap increases from 0.94 eV to 1.22 eV as strain increases from -7% to -1% (for compressive strain). The bandgap decreases from 1.04 eV to 0 eV as strain increases from 1% to 7% (for tensile strain).

Further, we analyzed the tunability of the bandgap with the strain (ΔEg/Δε), by linearly fitted the bandgap value in K to Σ_{min}, Γ-Σ_{min} and Γ-K of three regimes as displayed in table 5.1. For AB-$MoSe_2$ bilayer, in the strain range of -7 % to -1.9 % (K to Σ_{min}), the ΔEg/Δε is ~ 60.16 meV/ %; in the strain range of -1.8% to 0.04 % (Γ-Σ_{min}), the ΔEg/Δε is -46.7 meV/ % and in the strain range of 0.05% to 6% (Γ-K), the ΔEg/Δε is -148.25 meV/ %.

5.2 AA Stacking $MoSe_2$ bi-layer

Here, we have investigated the tunability of the electronic structure of AA-stacked bilayer $MoSe_2$ upon application of biaxial strain ($\varepsilon = \varepsilon x = \varepsilon y$). We notice that in modulating electronic properties the biaxial strain is the most effective compare to the uniaxial and shear strain. We varied the ε from -6 % to +6%, where + and – signs represent tensile and compressive strain.

First, we relaxed the AA-stacked bilayer $MoSe_2$ at the PBE level. We also found that the total energy decreases with tensile and compressive strain for AA-stacked $MoSe_2$ BL. All the lattice parameters, bond length, bandgap, total energy, and formation energy of AA-stacked $MoSe_2$ BL at strain varying from -6% to +6% have been shown in Table 5.2.

Table 5.2: The relaxed lattice constants (a), Interlayer distance ($d_{Se\text{-}Se}$), the bandgap, and total energy (Etot)of the system under different compressive and tensile strain conditions.

Strain(%)	Lattice Constant (Á)	Interlayer Distance(Á)	Bandgap (eV)	Bandgap transition	Total Energy(eV)
-6	3.12	3.761	1.08	K->Σ_{min}	-158.05021
-5	3.15	3.768	1.15	K->Σ_{min}	-158.25451
-4	3.18	3.774	1.21	K->Σ_{min}	-158.38896
-3	3.21	3.781	1.28	K->Σ_{min}	-158.53980
-2	3.25	3.787	1.34	K->Σ_{min}	-158.62481
-1	3.28	3.79	1.39	K->Σ_{min}	-158.67371
0	3.317	3.698	1.387	T->K	-158.74096
1	3.35	3.8	1.228	T->K	-158.66785
2	3.38	3.8	1.039	T->K	-158.61627
3	3.41	3.81	0.861	T->K	-158.53387
4	3.45	3.76	0.677	T->K	-158.41626
5	3.48	3.77	0.527	T->K	-158.27758
6	3.51	3.78	0	-	-158.11229

To further analyze, we have plotted bandgap variations of both AB-$MoSe_2$ BL and AA-$MoSe_2$ BL with biaxial strain in one plot, as shown in Fig. 5.3. From the plot, we observed that the bandgap energy linearly decreases with tensile strain and when we applied 6% Strain, for AA stacking bilayer $MoSe_2$ have been shown semiconductor to metallic transition.

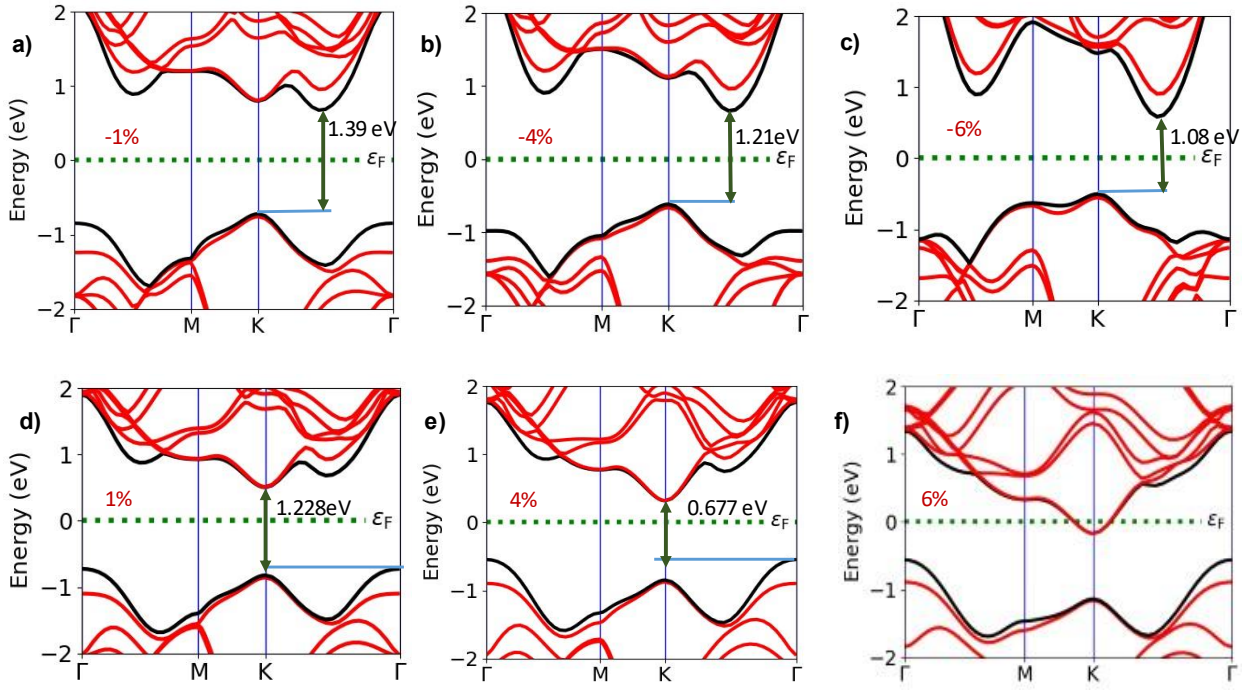

Fig5.2: Band diagram of AA stacking $MoSe_2$ bilayer for biaxial compressive and tensile strain at ε = (a) -1%, (b) -4%, (c) -6%, (d) 1%, (e) 4% and (f) 6%. The bandgap transition changes K-Σ_{min} (-6% - -0.05%) for compressive strain and Γ-K (0.05% - 5%) for tensile strain. The bandgap increases from 1.08 eV to 1.39 eV as strain increases from -6% to -1% (for compressive strain). The bandgap decreases from 1.228 eV to 0 eV as strain increases from 1% to 6% (for tensile strain).

Now, the tunability of the bandgap with the strain (ΔEg/Δε) determined by linearly fitting the bandgap value in compressive strain (K to Σmin) and tensile strain (Γ-K) regimes as displayed in table 5.2. For AA- $MoSe_2$ bilayer in the strain range of -6 % to -0.05 % (K to Σ_{min}), the ΔEg/Δε is ~ 59.47 meV/ %; in the strain range of 0.05 % to 5 % (Γ-K), the ΔEg/Δε is -168.17 meV/ %.

The bandgap's rate of tunability (ΔEg/Δε) in the tensile range is -168.17 meV/%, whereas for compressive range ~59.47 meV/% is higher in tensile strain. Finally, we compare the variation of band gap of AB and AA stacked 2L $MoSe_2$ with biaxial strain.

Fig. 5.3 compare the band gap values versus Biaxial strain for both AB and AA stacked bilayer $MoSe_2$.

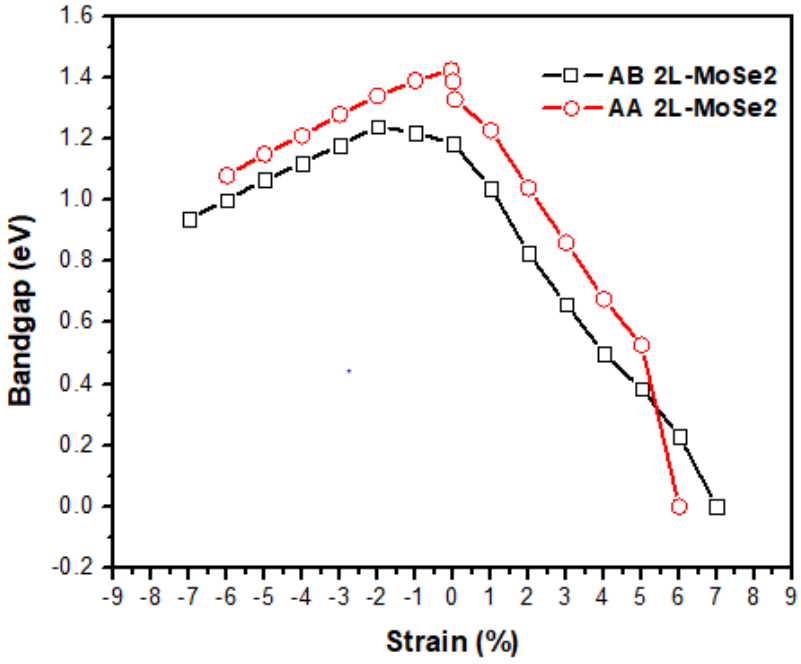

Fig 5.3: Bandgap variation of AB Stacking $MoSe_2$ bilayer with the biaxial strain from -7% to +7% and Bandgap variation of AA Stacking $MoSe_2$ bilayer with the biaxial strain from -6% to +6%.

Chapter -6

Conclusion and Future Scope

6.1 Conclusion

$MoSe_2$ monolayer is one of the most important 2D-TMDCs materials for electronics and optoelectronics application. As compare to monolayer, the bilayer $MoSe_2$ are particularly attractive for applications such as FETs, sensors, logic devices etc., due to its improved current carrying capacity, lower contact resistance and higher mobility. Therefore, in thesis work, we investigated variation in electronic structure of AB and AA stacked bilayer $MoSe_2$ under application of biaxial strain and external electric Field.

Chapter-1, presents some general aspects of TMDCs as a 2D material, particularly physical properties of one of the most important 2D-TMDC materials i.e., $MoSe_2$ discussed in details.
Also, we discussed about bilayer TMDCs and their stacking order mainly AB and AA discussed in details. Then, we discussed in details about different type of strain and fundamental and application of External Electric Field. Finally, we discussed in the details about DFT calculations in details.

Chapter-2 includes the review of some important state-of-the-art works reported on the electronics and optical characteristics of homo-bilayer $MoSe_2$. A detailed literature survey on the reported stacking order, effect of biaxial strain and effect of external electric field has been presented.

Chapter-3 In this chapter, we analyzed electronics and optical properties of 1L-$MoSe_2$ and 2L-$MoSe_2$ of AB and AA stacking order using QuantumATK software. We observed that the number of layers increases the bandgap starts decreasing and it changes from direct-bandgap to indirect-bandgap. We investigate that AA-stacking 2L-$MoSe_2$ have wider bandgap than AB-stacking 2L-

$MoSe_2$. If we see on value of binding energy then we observed that AB-stacking 2L-$MoSe_2$ is more energetically stable than AA-stacking 2L-$MoSe_2$.

Chapter-4 In this chapter, we investigated effect of external electric field on the electronic structure of bilayer $MoSe_2$ of AB and AA stacking order. Bandgap of AA stacking bilayer $MoSe_2$ (1.25 eV) is larger compared to AB stacking bilayer $MoSe_2$ (1.09 eV). Electronics property tuning capability of AA stacking bilayer $MoSe_2$ is faster than AB stacking bilayer $MoSe_2$. We observed that in AA stacking bilayer $MoSe_2$, bandgap is more but electronics behavior changing from semiconductor to metallic occurred in less applied electric field (2.2 eV) compared to AB stacking bilayer $MoSe_2$. Other side in AB stacking bilayer $MoSe_2$, bandgap is less but electronics behavior changing from semiconductor to metallic occurred in more applied electric field (2.8 eV) compared to AA stacking bilayer $MoSe_2$.Therefore, we conclude that AA stacking bilayer $MoSe_2$ is more sensitive than AB stacking bilayer $MoSe_2$.

Chapter-5 In this chapter, we analysed effect of biaxial strain on the electronic structure of AB and AA Bi-layer $Mose_2$**.** Under tensile strain, the bandgap decreses linearly with strain whereas for compressive strain the the bnadgap intially increses then further decreses in band gap value is observed for both AB and AA bilayer $MoSe_2$. Both the AB and AA-bilayer $MoSe_2$ shows semiconductor to metal transition at $\varepsilon \sim +6\%$. However, under compressive strain higher value of strain is required. We found that for indirect gap transition K to Σmin, the value of $\Delta Eg/\Delta\varepsilon$ is almost equal for both AB and AA stacking $MoSe_2$ BL. However, for transition Γ-K, the $\Delta Eg/\Delta\varepsilon$ value for AB- $MoSe_2$ BL < AA- $MoSe_2$ BL. This suggests that the bandgap of AA- $MoSe_2$ BL is more tunable than the AB- $MoSe_2$ BL.

6.2 Future scope

2D-Semiconducting TMDCs materials have been used in many electronics, optoelectronics and application areas such as photo detector, solar cell, light emitting diodes, sensors, photo transistors, piezoelectric devices etc. In this work, we did atomistic simulations of homobilayer $MoSe_2$ atomic structure of AB & AA stacking order and analyzed their electronics and optical properties. Also, we applied effect of electric field and biaxial strain on bilayer $MoSe_2$ of AB & AA stacking order and analyzed changes in electronics characteristics. For further work, we can analyze more characteristics on homobilayer $MoSe_2$ to get more information which is help for future reference in optoelectronics application, power electronics devices and optical devices and also, we can do similar work on other TMDC materials like WSe_2, WS_2, $MoTe_2$, MoS_2 etc. to explore more information about TMDC materials. By focusing on the tunable electronic structure, the scientific impact of 2D-semiconducting TMDCs can likely be maximized. This work's analysis and insights might be useful for interpreting experiments on 2L $MoSe_2$ and studying to guide future experimental work on AB and AA stacked 2L $MoSe_2$ based devices.

References

1. Jariwala, D., et al., *Emerging Device Applications for Semiconducting Two-Dimensional Transition Metal Dichalcogenides.* ACS Nano, 2014. **8**(2): p. 1102-1120.
2. Ścieżyńska, D., et al., *Two-Dimensional Nanostructures in the World of Advanced Oxidation Processes.* Catalysts, 2022. **12**.
3. Khan, K., et al., *Recent development in Graphdiyne and its derivative materials for novel biomedical applications.* Journal of Materials Chemistry B, 2021. **9**.
4. Li, X. and H. Zhu, *Two-dimensional MoS2: Properties, preparation, and applications.* Journal of Materiomics, 2015. **1**(1): p. 33-44.
5. Alam, S., et al., *Synthesis of emerging two-dimensional (2D) materials – Advances, challenges and prospects.* FlatChem, 2021. **30**: p. 100305.
6. Velický, M. and P.S. Toth, *From two-dimensional materials to their heterostructures: An electrochemist's perspective.* Applied Materials Today, 2017. **8**: p. 68-103.
7. Novoselov, K.S., et al., *2D materials and van der Waals heterostructures.* Science, 2016. **353**(6298): p. aac9439.
8. Ahmed, S. and J. Yi, *Two-Dimensional Transition Metal Dichalcogenides and Their Charge Carrier Mobilities in Field-Effect Transistors.* Nano-Micro Letters, 2017. **9**(4): p. 50.
9. Tian, H., et al., *Optoelectronic devices based on two-dimensional transition metal dichalcogenides.* Nano Research, 2016. **9**.
10. Chaves, A., et al., *Bandgap engineering of two-dimensional semiconductor materials.* npj 2D Materials and Applications, 2020. **4**(1): p. 29.
11. Glavin, N., et al., *Emerging Applications of Elemental 2D Materials.* Advanced Materials, 2020. **32**.
12. Phuc, H.V., et al., *First principles study of the electronic properties and band gap modulation of two-dimensional phosphorene monolayer: Effect of strain engineering.* Superlattices and Microstructures, 2018. **118**: p. 289-297.
13. Monga, D., et al., *Advances in transition metal dichalcogenide-based two-dimensional nanomaterials.* Materials Today Chemistry, 2021. **19**: p. 100399.
14. Wang, J., et al., *Optoelectronic and Photoelectric Properties and Applications of Graphene-Based Nanostructures.* Materials Today, 2020. **13**: p. 100193.
15. Vogel, E. and J. Robinson, *Two-dimensional layered transition-metal dichalcogenides for versatile properties and applications.* MRS Bulletin, 2015. **40**: p. 558-563.
16. Yadav, C. and Y. Chauhan, *Modeling of Transition Metal Dichalcogenide Transistors for SPICE Simulation at MOS-AK Workshop, Berkeley, Dec. 2016*. 2016.
17. Brent, J.R., N. Savjani, and P. O'Brien, *Synthetic approaches to two-dimensional transition metal dichalcogenide nanosheets.* Progress in Materials Science, 2017. **89**: p. 411-478.
18. Lv, R., et al., *Transition Metal Dichalcogenides and Beyond: Synthesis, Properties, and Applications of Single- and Few-Layer Nanosheets.* Accounts of chemical research, 2014. **48**.
19. Johari, P. and V. Shenoy, *Tuning the Electronic Properties of Semiconducting Transition Metal Dichalcogenides by Applying Mechanical Strains.* ACS nano, 2012. **6**: p. 5449-56.

20. Choi, W., et al., *Recent development of two-dimensional transition metal dichalcogenides and their applications.* Materials Today, 2017. **20**(3): p. 116-130.
21. Tsuneda, T., *Density Functional Theory in Quantum Chemistry*. Density Functional Theory in Quantum Chemistry, 2013: p. 1-200.
22. Baseden, K.A. and J.W. Tye, *Introduction to Density Functional Theory: Calculations by Hand on the Helium Atom.* Journal of Chemical Education, 2014. **91**(12): p. 2116-2123.
23. Gerlach, C., M. Murillo, and L. Stanton, *Hydrodynamic Density Functional Theory of Dense, Heterogeneous Plasmas*. 2021. p. NP11.123.
24. van Mourik, T., M. Bühl, and M.-P. Gaigeot, *Density functional theory across chemistry, physics and biology.* Philosophical transactions. Series A, Mathematical, physical, and engineering sciences, 2014. **372**(2011): p. 20120488-20120488.
25. Ugeda, M.M., et al., *Giant bandgap renormalization and excitonic effects in a monolayer transition metal dichalcogenide semiconductor.* Nature Materials, 2014. **13**(12): p. 1091-1095.
26. Tongay, S., et al., *Thermally Driven Crossover from Indirect toward Direct Bandgap in 2D Semiconductors: MoSe2 versus MoS2.* Nano Letters, 2012. **12**(11): p. 5576-5580.
27. Gusakova, J., et al., *Electronic Properties of Bulk and Monolayer TMDs: Theoretical Study Within DFT Framework (GVJ-2e Method).* physica status solidi (a), 2017. **214**(12): p. 1700218.
28. He, J., K. Hummer, and C. Franchini, *Stacking effects on the electronic and optical properties of bilayer transition metal dichalcogenides MoS_2, $MoSe_2$, WS_2 and WSe_2.* Phys. Rev. B, 2014. **89**(7): p. 075409.
29. Xia, M., et al., *Spectroscopic Signatures of AA' and AB Stacking of Chemical Vapor Deposited Bilayer MoS2.* ACS Nano, 2015. **9**(12): p. 12246-12254.
30. Zhang, X., et al., *Transition metal dichalcogenides bilayer single crystals by reverse-flow chemical vapor epitaxy.* Nature Communications, 2019. **10**(1): p. 598.
31. Peng, G., et al., *Controllable Epitaxial Growth of MoSe2 Bilayers with Different Stacking Orders by Reverse-Flow Chemical Vapor Deposition.* ACS Applied Materials & Interfaces, 2020. **12**(20): p. 23347-23355.
32. Kumar, A. and P.K. Ahluwalia, *Semiconductor to metal transition in bilayer transition metals dichalcogenidesMX2(M= Mo, W;X= S, Se, Te).* Modelling and Simulation in Materials Science and Engineering, 2013. **21**(6): p. 065015.
33. He, J., K. Hummer, and C. Franchini, *Stacking effects on the electronic and optical properties of bilayer transition metal dichalcogenides ${\mathrm{MoS}}_{2}$, ${\mathrm{MoSe}}_{2}$, ${\mathrm{WS}}_{2}$, and ${\mathrm{WSe}}_{2}$.* Physical Review B, 2014. **89**(7): p. 075409.
34. Ross, J.S., et al., *Electrical control of neutral and charged excitons in a monolayer semiconductor.* Nature Communications, 2013. **4**(1): p. 1474.
35. Fiori, G., et al., *Electronics based on two-dimensional materials.* Nat. Nanotechnol., 2014. **9**: p. 768.
36. Chuang, S., et al., *MoS2 P-type Transistors and Diodes Enabled by High Work Function MoOx Contacts.* Nano Letters, 2014. **14**(3): p. 1337-1342.
37. Fang, H., et al., *High-Performance Single Layered WSe2 p-FETs with Chemically Doped Contacts.* Nano Letters, 2012. **12**(7): p. 3788-3792.
38. Kiriya, D., et al., *Air-Stable Surface Charge Transfer Doping of MoS2 by Benzyl Viologen.* Journal of the American Chemical Society, 2014. **136**(22): p. 7853-7856.

39. Yang, L., et al., *Chloride Molecular Doping Technique on 2D Materials: WS2 and MoS2.* Nano Letters, 2014. **14**(11): p. 6275-6280.
40. Liu, X., et al., *P-Type Polar Transition of Chemically Doped Multilayer MoS2 Transistor.* Advanced Materials, 2016. **28**(12): p. 2345-2351.
41. Somvanshi, D., et al., *Improved Current Density and Contact Resistance in Bilayer $MoSe_2$ Field Effect Transistors by AlO_x Capping.* ACS Appl. Mater. Interfaces, 2020. **12**(32): p. 36355-36361.
42. Zhang, L., et al., *Tuning Electrical Conductance in Bilayer MoS2 through Defect-Mediated Interlayer Chemical Bonding.* ACS Nano, 2020.
43. Li, H., et al., *Fabrication of Single- and Multilayer MoS_2 Film-Based Field-Effect Transistors for Sensing NO at Room Temperature.* Small, 2012. **8**(1): p. 63-67.
44. Conley, H.J., et al., *Bandgap Engineering of Strained Monolayer and Bilayer MoS2.* Nano Letters, 2013. **13**(8): p. 3626-3630.
45. Zhuang, H.L. and R.G. Hennig, *Computational Discovery, Characterization, and Design of Single-Layer Materials.* JOM, 2014. **66**(3): p. 366-374.
46. Hu, X., L. Kou, and L. Sun, *Stacking orders induced direct band gap in bilayer MoSe2-WSe2 lateral heterostructures.* Sci Rep, 2016. **6**: p. 31122.
47. Ma, Y., et al., *Effect of an external electric field on the electronic properties of SnS2/PbI2 van der Waals heterostructures.* RSC Advances, 2017. **7**(41): p. 25582-25588.
48. Cortés, N., et al., *Stacking change in MoS(2) bilayers induced by interstitial Mo impurities.* Scientific reports, 2018. **8**(1): p. 2143-2143.
49. Deng, S., L. Li, and M. Li, *Stability of direct band gap under mechanical strains for monolayer MoS2, MoSe2, WS2 and WSe2.* Physica E: Low-dimensional Systems and Nanostructures, 2018.
50. Xiao, X.-B., et al., *Electric Field Controlled Indirect-Direct-Indirect Band Gap Transition in Monolayer InSe.* Nanoscale Research Letters, 2019. **14**(1): p. 322.
51. Somvanshi, D., et al., *Improved Current Density and Contact Resistance in Bilayer MoSe2 Field Effect Transistors by AlOx Capping.* ACS Applied Materials & Interfaces, 2020. **12**(32): p. 36355-36361.
52. Guo, J., et al., *Strain Engineering on the Electronic and Optical Properties of WSSe Bilayer.* Nanoscale Research Letters, 2020. **15**(1): p. 97.
53. Peng, Z., et al., *Strain engineering of 2D semiconductors and graphene: from strain fields to band-structure tuning and photonic applications.* Light: Science & Applications, 2020. **9**(1): p. 190.
54. Postorino, S., et al., *Strain-induced effects on the electronic properties of 2D materials.* Nanomaterials and Nanotechnology, 2020. **10**: p. 1847980420902569.
55. Ghosh, S.K. and D. Somvanshi, *First-principal insight of the gold-metal interaction to bilayer MoSe2 of AB and AA stacking order.* Solid State Communications, 2022. **342**: p. 114613.
56. Guan, X., et al., *Tuning the electronic properties of monolayer MoS2, MoSe2 and MoSSe by applying z-axial strain.* Chemical Physics Letters, 2019. **730**: p. 191-197.
57. Hu, X., L. Kou, and L. Sun, *Stacking orders induced direct band gap in bilayer MoSe2-WSe2 lateral heterostructures.* Scientific Reports, 2016. **6**(1): p. 31122.
58. Carrascoso, F., et al., *Strain engineering in single-, bi- and tri-layer MoS2, MoSe2, WS2 and WSe2.* Nano Research, 2021. **14**(6): p. 1698-1703.

59. Kumar, A. and P. Ahluwalia, *Semiconductor to metal transition in bilayer transition metals dichalcogenides MX2 (M = Mo, W; X = S, Se, Te).* Modelling and Simulation in Materials Science and Engineering, 2013. **21**: p. 065015.
60. Liu, K., et al., *Evolution of interlayer coupling in twisted molybdenum disulfide bilayers.* Nature Communications, 2014. **5**(1): p. 4966.
61. Smidstrup, S., et al., *QuantumATK: an integrated platform of electronic and atomic-scale modelling tools.* Journal of Physics: Condensed Matter, 2019. **32**(1): p. 015901.
62. Deng, S., L. Li, and M. Li, *Stability of direct band gap under mechanical strains for monolayer MoS2, MoSe2, WS2 and WSe2.* Physica E: Low-dimensional Systems and Nanostructures, 2018. **101**: p. 44-49.
63. Horng, J., et al., *Observation of interlayer excitons in ${\mathrm{MoSe}}_{2}$ single crystals.* Physical Review B, 2018. **97**(24): p. 241404.
64. Hoat, D., et al., *Tuning the Electronic Structure of 2D Materials by Strain and External Electric Field: Case of GeI2 Monolayer.* Chemical Physics, 2019. **527**: p. 110499.
65. Ahmad, S., *Strain and electric field dependent variation in electronic and thermoelectric properties of PtS2.* Results in Physics, 2020. **17**: p. 103088.
66. Zeng, J., et al., *Effects of Strain and Electric Field on Molecular Doping in MoSSe.* ACS Omega, 2021. **6**(22): p. 14639-14647.
67. Zhang, D., et al., *Tunable Electric Properties of Bilayer α-GeTe with Different Interlayer Distances and External Electric Fields.* Nanoscale Research Letters, 2018. **13**(1): p. 400.
68. Yang, S., Y. Chen, and C. Jiang, *Strain engineering of two-dimensional materials: Methods, properties, and applications.* InfoMat, 2021. **3**.